File with N76-31451

DIVISION OF CIVIL AND MECHANICAL ENGINEERING

ROSE-HULMAN INSTITUTE OF TECHNOLOGY

REPORT ME 76-1-ATR:

Turbulent Boundary Layers Over Nonstationary Plane Boundaries

A. T. Roper

Study supported by the National
Aeronautics and Space Administration
Under NASA Grant: NSG 1258

Terre Haute, Indiana

September, 1976

ABSTRACT

Methods of predicting integral parameters and skin-friction coefficients of turbulent boundary layers developing over moving-ground-planes are evaluated using test information from three different wind tunnel facilities at the NASA Langley Research Center. These data include test information from the VSTOL tunnel which is presented for the first time. The three methods evaluated are

(1) Relative integral parameter method

(2) Relative power law method

(3) Modified law of the wall method

Methods (1) and (2) can be used to predict moving-ground-plane shape factors with an expected accuracy of $\pm 10\%$. They may also be used to predict moving-ground-plane displacement and momentum thicknesses with lower expected accuracy. This decrease in accuracy can be traced to the failure of approximations upon which these methods are based to prove universal when compared with VSTOL tunnel test results.

While no attempt is made to establish the accuracy of the local skin-friction coefficients predicted by the various methods, those produced by methods (1) and (2) show a high degree of agreement. The modified law of the wall method predicts a more rapid decrease in skin-friction with increasing ratio of ground-plane to free-stream velocity than do methods (1) and (2).

TURBULENT BOUNDARY LAYERS OVER NONSTATIONARY PLANE BOUNDARIES

by Alan T. Roper* and Garl L. Gentry, Jr.
Langley Research Center

SUMMARY

Methods of predicting integral parameters and skin-friction coefficients of turbulent boundary layers developing over moving-ground-planes are evaluated using test information from three different wind tunnel facilities at the NASA Langley Research Center. These data include test information from the VSTOL tunnel which is presented for the first time. The three methods evaluated are

(1) Relative integral parameter method

(2) Relative power law method

(3) Modified law of the wall method

Methods (1) and (2) can be used to predict moving-ground-plane shape factors with an expected accuracy of $\pm$10%. They may also be used to predict moving-ground-plane displacement and momentum thicknesses with lower expected accuracy. This decrease in accuracy can be traced to the failure of approximations upon which these methods are based to prove universal when compared with VSTOL tunnel test results.

While no attempt is made to establish the accuracy of the local-skin friction coefficients predicted by the various methods, those produced by methods (1)

---

*Professor, Division of Civil and Mechanical Engineering, Rose-Hulman Institute of Technology, Terre Haute, Indiana, 47803.

and (2) show a high degree of agreement. The modified law of the wall method predicts a more rapid decrease in skin friction with increasing ratio of ground-plane to free-stream velocity than do methods (1) and (2).

INTRODUCTION

Turbulent boundary layer flows developing over nonstationary boundaries are of interest in studies related to a variety of flows including the Ludweig Tube, moving shock waves near solid boundaries and the near field drag of tube vehicles. It is thus desirable to determine methods for predicting the values of the various integral parameters as well as the skin-friction coefficient for such boundary-layer flows.

Since all present methods of turbulent-boundary-layer calculation rely upon empirical information, and since no significant body of such information exists for the moving-ground-plane case, any useful method of prediction must originate from stationary-ground-plane methods. Three such methods, the

(1) Relative integral parameter method

(2) Relative power law method

(3) Modified law of the wall method

have been proposed and partially varified by tests performed in two NASA Langley Research Center wind tunnels equipped with moving ground belts. The bulk of this test information was obtained at $R_x < 2 \times 10^6$. In an effort to extend the Reynolds number range and complete the varification of one or more of the proposed methods, tests were conducted in the NASA Langley Research Center VSTOL tunnel at Reynolds numbers up to 9.2×10^6. The results of this latest series of tests are analyzed, compared to those of previous tests and presented in this report.

SYMBOLS

The units used for physical quantities in this report are given in both the International System of Units (SI) and the U.S. Customary Units. Measurements and calculations were made in the U.S. Customary Units.

A, B, A', B'	empirically determined constants
C_f	total skin-friction coefficient
$C_f(0)$	stationary-ground-plane total skin-friction coefficient
c_f	local skin-friction coefficient
$c_f(0)$	stationary-ground-plane local skin-friction coefficient
g(R)	empirically determined polynomial
H	shape factor
H(0)	stationary-ground-plane shape factor
N	reciprocal of power in relative power law formulation, n(R=0)
n	reciprocal of power in power law formulation
R	velocity ratio (nominal value) V_B/U
R_x	Reynolds number based on x
R_y	Reynolds number based on y and U
U	x-component of mean velocity at edge of boundary layer, meters/sec. (feet/second)
u	local x-component of mean velocity, meters/second (feet/second)
u	friction velocity, $\sqrt{\tau_0/\rho}$ meters/second (feet/second)
V_B	velocity of ground belt, meters/second (feet/second)
x	longitudinal distance from leading edge of ground belt, meters (feet)

y	vertical distance from ground belt, centimeters (inches)
δ	boundary-layer thickness, centimeters (inches)
$\delta(0)$	stationary-ground-plane boundary-layer thickness
δ^*	displacement thickness, $\int_0^\infty (1-u/U)\,dy$, centimeters (inches)
$\delta^*(0)$	stationary-ground-plane displacement thickness, centimeters (inches)
ε	an error
η	reciprocal of the exponent in the modified Blasius shear-stress formulation
θ	momentum thickness, $\int_0^\infty (u/U)(1-u/U)\,dy$, centimeters (inches)
$\theta(0)$	stationary-ground-plane displacement thickness, centimeters (inches)
μ	dynamic viscosity, newton-seconds/ meter^2 (lbf-sec/ft^2)
ρ	mass density, kilograms/meter^3 (slugs/foot^3)
τ	shearing stress, newtons/meter^2 (pounds force/foot^2)

Subscript:

o	measured at y = 0

A tilde ($\sim$) over a symbol indicates a relative velocity or a quantity based upon velocity measured relative to the ground plane; for example,

$$\tilde{\delta}^* = \int_0^\infty (1 - \tilde{u}/\tilde{U})\,dy$$

ANALYSIS

Experimental Data

The data analyzed and presented for the first time in this report were obtained in the VSTOL wind tunnel at the Langley Research Center. The tunnel was

fitted with a moving smooth-surfaced ground belt (representing a moving-ground plane) and operated with the tunnel side walls in place. Slots fitted in the side walls to allow variable porosity were, however, partially opened. Velocity profiles were measured by means of a total-pressure rake composed of forty-six (46) separate tubes of 0.127 centimeters (0.05 inches) diameter. Simultaneous static pressure measurements were made by means of a separate probe located to one side of the rake and at a nominal height of 4.2 centimeters (1.65 inches) above the ground belt. The general arrangement of the total pressure rake is shown in figure 1. All pressure data were recorded directly on magnetic tape using a rotary valve and pressure transducer arrangement.

The empirical data presented from all three tests were obtained in wind tunnel facilities equipped with porous suction plates to remove the normal tunnel boundary layer; therefore layers presented in this report are assumed to originate at the leading edge of the belt. In practice, however, it was not possible in any of the three tunnels to remove the entire tunnel boundary layer. The effects of this incomplete boundary-layer removal are shown for the R=1.0 (nominal) profiles taken in the VSTOL facility in figure 2. These profiles represent somewhat better removal capability than that of the tunnels used in references 1 and 2. Additional disturbances were caused in all three sets of data at the leading edge by the small slot (between the suction plate and the belt) and the natural entrainment of air from this slot by the belt motion. Further inaccuracies were encountered for readings taken nearest the belt because of the tendency of the belts to lift slightly when in motion. None of the data are corrected for these disturbances.

Total pressure measurements were made at a nominal dynamic pressure of 526.68 N/m^2 (11 lbf/ft^2), velocity of 29.26 m/sec (96.00 ft/sec), and Reynolds number per

unit length of 1.87×10^6 per meter (5.70×10^6 per foot) at stations 1.37 m (4.50 ft), 2.62 m (8.58 ft), 3.35 m (11.00 ft), 4.27 m (14.00 ft), and 5.18 m (17.00 ft) aft of the belt leading edge. Tunnel static pressure during testing was nominally atmospheric. For these conditions, the range of test Reynolds numbers was $2.62 \times 10^6 \leq R_x \leq 9.21 \times 10^6$. Data were recorded at values of V_B/U of approximately 0,0.24,0.48, 0.74, and 1.00.

Throughout the test a periodic unsteadiness in the boundary layer of as much as $\pm$ 0.76 m/sec ($\pm$2.5 ft/sec) was noted in the velocity measurements. No such fluctuations were apparent in the high velocity central core of the test section where tunnel center line velocity varied less than $\pm$ 0.15 m/sec ($\pm$ 0.50 ft/sec) during any given test. Efforts to find and eliminate the source of the unsteadiness were unsuccessful. In an effort to eliminate errors induced by this flow condition, multiple readings were taken of all pressure measurements as summerized in table I. Velocities quoted in this report are the arithmetic average of the velocities determined for each of the multiple pressure measurements. This scheme was not totally satisfactory and some of the scatter apparent in the measured velocity profiles is undoubtedly attributable to this source.

Velocity profiles measured during the VSTOL tunnel tests are presented in figures 3(a) to 3(e) in ln-ln form; the velocity data are also given in table II. Summaries of the boundary-layer thickness δ and the integral parameters δ^*, θ, and H determined from the measured data are presented in table III. The variation of the boundary-layer thickness with V_B/U is presented in figure 4. Also displayed in that figure are results from references 1 and 2.

Theoretical Methods

Brief descriptions are presented of the three methods which have been suggested [1,2] for predicting the development of the turbulent boundary layer over a

moving-ground-plane. Evaluation of each method is accomplished by comparison with data measured during the VSTOL tunnel tests and, where appropriate, data from references 1 and 2 are included.

Relative integral parameter method.[1,2] - This method is based upon developing expressions for the relative integral parameters, $\tilde{\delta}^*$, $\tilde{\theta}$, and $\tilde{H}$ by replacing the variable u/U in the usual parameter definitions by

$$\frac{\tilde{u}}{\tilde{U}} = \frac{u - V_B}{U - V_B} = \frac{u/U - R}{1 - R} \tag{1}$$

Thus, for example

$$\tilde{\delta}^* = \int_0^\infty \left(1 - \frac{\tilde{u}}{\tilde{U}}\right) dy$$

If the following assumptions are adopted

(1) $\tilde{H}$ is nearly independent of R

(2) $\theta/\theta(0)$ is some function independent of x, say g(R)

expressions relating stationary and moving-ground-plane integral parameters can be generated

$$\theta = g(R)\,\theta(0) \tag{2}$$

$$\delta^* = \frac{H(0)}{1 + R[H(0) - 1]}\, g(R)\,\theta(0) \tag{3}$$

$$H = \frac{H(0)}{1 + R[H(0) - 1]} \tag{4}$$

where g(R) is obtained by fitting the measured data.

The accuracy of this method rests ultimately upon the validity of assumptions (1) and (2). Of these two assumptions, the first is the least critical.

Errors in predicted values of H/H(0) resulting from deviations in the assumed relation $\tilde{H}/H(0) = 1$ can be expressed as

$$\mathcal{E}(H/H(0)) = \pm \left| \frac{1-R}{[1+R(\tilde{H}-1)^2]} \right| \left| \mathcal{E}(\tilde{H}/H(0)) \right| \qquad (5)$$

The variation of $\tilde{H}/H(0)$ as a function of R is presented in figure 5 for all three sets of test data. It will be noted that assumption (1) is rather seriously violated ($\mathcal{E}(\tilde{H}/H(0)$ maximum of the order of $\pm.25$) and that the maximum variations correspond to large values of R. However, as the first term of equation (5) is always less than one, it serves to attenuate errors resulting from assumption (1). Further, the magnitude of that attenuation grows with increasing values of R. For data in this report, maximum errors in H/H(0) resulting from the assumption $\tilde{H}$=H(0) are no more than $\pm$8%. These errors correspond to mid-range values of R. Errors in the determination of $\tilde{H}/H(0)$ also enter into the determination of $\delta^*/\delta^*(0)$ (equation 3).

The accuracy of assumption (2) is more critical as it enters directly (unattenuated) into both the determination of $\theta/\theta(0)$ and $\delta^*/\delta^*(0)$ (equations (2) and (3)). Reference 2 suggested that g(R) could be represented adequately by the expression

$$g(R) = (1-R)\left[1 - 1.1756R + 0.7863R(1+R)\right] \qquad (6)$$

The variation predicted by equation (6) is displayed in figure 6 together with data from this report and references 1 and 2. The expression appears to be a reasonable representation of the data, although a greater x-dependence is apparent in the current data than in that of either of the previous tests. Scatter about the predicted variation indicates a spread of approximately $\pm$0.10 which is

nearly uniform across the R range. Some of this scatter is undoubtedly due to the unsteadiness noted in the boundary-layer velocities of the VSTOL tests.

Measured values of H/H(0), θ/θ(0) and $\delta^*/\delta^*(0)$ are compared with those predicted from equations (3), (4) and (5) in figures 7(a) to 7(e). Correlations between measured and predicted values of H/H(0) are good with the maximum error being less than 8%. Correlations for $\delta^*/\delta^*(0)$ and θ/θ(0) are less good reflecting the scatter apparent in g(R) (figure 6).

The additional assumption that $c_f/c_f(0)$ like $\theta/\theta(0) = C_f/C_f(0)$ is independent of x allows the local skin-friction coefficients for the stationary and moving-ground-plane flows to be related.

Relative power law method[2] - The power law depicts the velocity within the boundary layer as

$$\frac{u}{U} = \left(\frac{y}{\delta}\right)^{1/n} \tag{7}$$

where n is a parameter somewhat dependent upon Reynolds number. Examination of existing moving-ground-plane boundary-layer measurements[1,2] led Roper and Gentry[2,3] to conclude that velocity distributions measured relative to a moving boundary admit to a similar formulation,

$$\frac{\tilde{u}}{\tilde{U}} = \left(\frac{y}{\tilde{\delta}}\right)^{1/N} \tag{8}$$

where N is nearly independent of V_B/U. While data from the current series of tests display more scatter than those of earlier tests[2], they conform sufficiently to the format suggested by equation (8) to corroborate its validity (figures 8(a) to 8(e).

Slopes of all measured profiles (VSTOL tunnel tests, reference 1, and reference 2) are summarized in figure 9 in the forms suggested by both equations (7)

and (8). It is important to note that while n is strongly dependent V_B/U, N is nearly constant. The primary motivation for the power law formulation is its simplicity. To maintain that simplicity, it appears desirable to set N = N(0) and to accept the resulting inaccuracy implied by the slight V_B/U dependence apparent in figure 9.

The usual integral parameters can be developed using their respective definitions and equation (8)

$$\delta^* = \left[(1-R)\left(\tilde{\delta}/\delta(0)\right)\right] \delta^*(0) \tag{9}$$

$$\Theta = \left[(1-R)\left(\frac{N+2R}{N}\right)\left(\tilde{\delta}/\delta(0)\right)\right] \Theta(0) \tag{10}$$

$$H = \left(\frac{N+2R}{N}\right) H(0) \tag{11}$$

Once stationary-ground-plane integral parameters have been computed, equations (9), (10), and (11) can be used to predict the corresponding moving-ground-plane values provided a suitable expression for $\tilde{\delta}/\delta(0)$ can be developed. Measured values for $\tilde{\delta}/\delta(0)$ are presented for all three sources in figure 10. A good deal of scatter is apparent, particularly at large values of V_B/U. The scatter is undoubtedly due partially to the inherent difficulty in determining $\tilde{\delta}$ and δ accurately, and, for the latest series of tests, is aggravated by the unsteadiness encountered in the boundary layer.

Measured values of $\tilde{\delta}/\delta(0)$ and the values of N(0) obtained from least-squares fits of the stationary-ground-plane logarithmic profiles were used with equations (9), (10), and (11) to compute $\delta^*/\delta^*(0)$, $\theta/\theta(0)$, and $H/H(0)$. These predicted values are compared with the experimentally determined ratios in figures

11(a) to 11(c). Correlations appear to be uninspiring but acceptable and display increasing accuracy of prediction as the longitudinal distance from the belt leading edge increases.

For incompressible turbulent flow past a semi-infinite flat plate, Blasius gives the variation of τ_o with δ to be

$$\frac{\tau_o}{\rho U^2} = 0.0225 \left(\frac{\mu}{\rho U \delta}\right)^{1/4} \qquad (12)$$

Extending equation (12) to include relative velocity[5], replacing 1/4 by $1/\eta$, and rearranging yields the expression for local skin-friction coefficient[2]

$$c_{f/2} = \frac{\tau_o}{\rho U^2} = 0.0225(1-R)^{\frac{2\eta-1}{\eta}} \left(\frac{\mu}{\rho U \delta}\right)^{1/\eta} \qquad (13)$$

where $R \leq 1$. Equation (13) can be used to predict local skin-friction coefficient for moving-ground-plane flows once the parameter η has been determined. Substitution of equation (13) into the integral form of the momentum equation for a flat-plate-zero-pressure-gradient boundary layer, integration, and rearrangement of the results produces the expression

$$\Sigma = \left(\frac{0.0225}{\Theta/\delta}\,\frac{\eta+1}{\eta}\right)^{\eta/\eta+1} (1-R)^{\frac{2\eta-1}{\eta+1}} \left(\frac{1}{R_x}\right)^{\frac{1}{\eta+1}} X \qquad (14)$$

Using measured values of δ and Θ/δ, and appropriate values of the various test conditions, equation (14) can be solved numerically for the various values of η. These results are presented in figure (12) for the latest series of tests and those of reference (2). The variation of $\eta/\eta(0)$ from both series of tests is consistent. Equation (14) was solved for c_f using computed values of η. The resulting local skin-friction coefficients are presented in figure 13 together with data from reference 2. With the exception of a single data point from the latest tests, scatter in the prediced value of c_f as a function of V_B/U is less than $\pm$13%.

Modified law of the wall method[2] - The final approach suggested in reference 2 is based upon the hypothesis that the relative velocity profiles obey the law of the wall in the modified form

$$\frac{\tilde{u}}{\tilde{u}_\tau} = A \log\left(\frac{\rho y \tilde{u}_\tau}{\mu}\right) + B \tag{15}$$

where

$$A = 5.75 \quad , \quad B = 5.20$$

and

$$\tilde{u}_\tau = \sqrt{\frac{\tau_0}{\rho}} = \tilde{U}\sqrt{\tilde{c}_{f/2}} \tag{16}$$

The local skin-friction coefficient based upon absolute velocity is related to that based upon relative velocity by the equation

$$c_{f/2} = (1-R)^2 \tilde{c}_{f/2} \tag{17}$$

Adopting the formulation suggested by Clauser[6], equation (15) can be rewritten as

$$\frac{\tilde{u}}{\tilde{U}} = A' \log(\tilde{R}_y) + B' \tag{18}$$

where A' and B' are functions of A, B, and c_f. Charts constructed for a range of $\tilde{c}_f$ values using equation (17) and measured data from the latest series of tests are presented in figures 14(a) to 14(e). Comparison of measured data with the computed $\tilde{c}_f$ grid is used to determine the value of relative skin-friction coefficient.

Although some of the profiles lack a clearly defined linear portion, it was nonetheless possible to determine approximate values of $\tilde{c}_f$ for all stations except x = 2.62 m (8.58 ft). Values of c_f determined in the manner

just outlined are presented in figure 15. Also displayed in that figure are the results reported in reference 2. Correlation between results for the two sets of measured data is good with maximum scatter being less than $\pm 6\%$.

Comparison of Local Skin-Friction Coefficient

The relative integral parameter method, relative power law, and modified law of the wall methods all yield means for predicting local skin-friction coefficient. The local skin-friction coefficient is an extremely difficult quantity to measure directly over a moving-ground-plane and no attempt has been made to establish the accuracy of the various methods. They are, however, compared in figure 16 (as a function of $\Theta/\Theta(0)$). Results from both the latest series of tests and those presented in reference 2 are displayed in that figure. Note that predictions of the relative integral parameter and power law methods agree within less than $\pm 6\%$. Values of c_f predicted by the modified law of the wall method are generally less than those of the other methods.

COMPARISONS OF PREDICTED AND MEASURED INTEGRAL PARAMETERS

In this section comparisons will be made of measured values of $\bar{\sigma}^*/\bar{\sigma}^*(0)$, $\Theta/\Theta(0)$, and H/H(0) with those predicted by the relative integral parameter and power law methods. Where available, data from all three existing sets of empirical measurements will be displayed.

H/H(0). - The expressions developed in the relative integral parameter and relative power law methods are

$$H = \frac{H(0)}{1 + R[H(0) - 1]} \tag{4}$$

and

$$H = \frac{N + 2}{N + 2R} \tag{11}$$

respectively. The first expression contains the approximations that $\tilde{H} = H(0)$, while the second approximates the actual value of N by N(0).

The accuracy of equations (4) and (11) is displayed in figure 17 by plotting predicted vs measured values of H/H(0). Lines indicating ±10% error are included on that figure. The relative integral parameter method is the somewhat more accurate of the two methods yielding errors from - 9% to 2%. This method generally somewhat underestimates the actual value of the ratio H/H(0). With the exception of four measurements from the current set of tests, the relative power law yields errors from - 3% to 13%. The power law method generally overestimates values of H/H(0).

$\Theta/\Theta(0)$. - The expressions developed in the relative integral parameter and relative power law methods are

$$\Theta/\Theta(0) = g(R) = (1-R)\left[1 - 1.1756R + 0.7563R(1+R)\right] \qquad (2), (5)$$

and

$$\Theta/\Theta(0) = (1-R)\left(\frac{N+2R}{N}\right)\tilde{\delta}/\delta(0) \qquad (10)$$

where values of $\tilde{\delta}/\delta(0)$ are taken from a curve fitted to the measured data in figure 10. For convenience, that curve is reproduced in figure 18.

Once again, the accuracy of equations (2), (5) and equation (10) is depicted by plotting measured vs predicted values of the ratio $\theta/\theta(0)$ (figure 19). Lines representing ±10% and ±20% errors are included on that figure. Of the two methods, the relative integral parameter method appears most accurate with 80% of the predicted points involving errors of ±20% or less and nearly 50% of the predictions falling within ±10% of the measured value. For the relative power

law method, 56% of the predicted values are within ±20% and 38% within ±10% of the measured values.

The accuracy of the proposed methods in the determination of $\Theta/\Theta(0)$ deteriorates markedly from that displayed in the prediction of H/H(0) (figure 17). This is due in large part to the failure of the empirical expressions for g(R) and $\tilde{\delta}/\delta(0)$ to accurately represent the experimental data. For the relative power law predictions, the situation is further aggravated by the approximation that $N \simeq N(0)$.

$\delta^*/\delta^*(0)$. - The expressions developed in the relative integral parameter and relative power law methods are

$$\delta^*/\delta^*(0) = \frac{H(0)}{1+R(H(0)-1)}\, g(R)\, \frac{\Theta(0)}{\delta^*(0)} = \frac{g(R)}{1+R(H(0)-1)} \qquad (2)$$

and

$$\delta^*/\delta^*(0) = (1-R)\,\tilde{\delta}/\delta(0) \qquad (9)$$

where, once again, values of $\tilde{\delta}/\delta(0)$ are taken from a curve fitted to the measured values of that parameter (figures 10 and 18).

The accuracy of equations (2) and (9) is depicted by plotting measured vs predicted values of the ratio $\delta^*/\delta^*(0)$ (figure 20). Lines representing ±10% and ±20% errors are included on that figure. Each of the two equations predict 60% of the measured data points within errors of less than or equal to ±20%. The relative power law method predicts 34% of the data points within errors of less than or equal to ±10% while the integral parameter method predicts only 26% within this error band. Overall, there is less dispersion of the error chart data than that displayed in the $\Theta/\Theta(0)$ chart (figure 19). Once again, the lack of an accurate match between measured data and the empirical formulations for g(r) and $\tilde{\delta}/\delta(0)$ seems to be the major source of error.

CONCLUSIONS

The validity of the proposed methods is somewhat clouded by the data scatter apparent primarily in the current series of tests. This scatter may be a result of the unsteadiness noted in the boundary-layer velocity measurements for which no explanation is advanced. Nevertheless, the following conclusions appear justified as a result of this investigation.

1. The velocity profiles measured near the ground plane in an incompressible turbulent boundary layer can be described by a relative power law formulation of the form

$$\tilde{u}/\tilde{U} = \left(y/\tilde{\delta}\right)^{1/N}$$

where $\tilde{u}/\tilde{U}$ is the ratio of velocities relative to the ground plane, $\tilde{\delta}$ is the relative boundary-layer thickness, y is the vertical distance from the ground plane, and N the slope of the stationary-ground-plane profile. This appears to be a particularly strong statement inasmuch as both smooth-belt boundary layers which are near transition (NASA TN D-6788) and more fully developed turbulent layers over rough-belts (NASA TM X-2515) and smooth-belts (the present study) admit to this description.

2. Either the relative integral parameter or the relative power law methods can be used to predict the ratio H/H(0) with an accuracy of approximately $\pm$10%.

3. Existing test information indicates that values of $\delta^*/\delta^*(0)$ and $\theta/\theta(0)$ predicted by either the relative integral parameter or power law method have a probability between 0.6 and 0.8 of errors of $\pm$20% or less. The reduction in

accuracy from that of H/H(0) predictions is due to the failure of empirical formulations for $\Theta/\Theta(0)$ (relative integral parameter) and $\delta^*/\delta^*(0)$ (relative power law) to prove universal, or nearly so, when compared to data from the latest series of tests.

4. While no statement can be made concerning their accuracy, there is a high degree of correlation between values of $c_f/c_f(0)$ predicted as a function of $\Theta/\Theta(0)$ by both the relative integral and relative power law methods.

5. The modified law of the wall method predicts a more rapid decrease in local skin-friction coefficient with increase in belt velocity to free-stream velocity ratio than do the relative integral parameter or relative power law methods.

Rose-Hulman Institute of Technology

Terre Haute, Indiana

September 13, 1976

REFERENCES

1. Roper, Alan T.; and Gentry, Garl L., Jr.: Analysis of a Turbulent Boundary Layer Over a Moving Ground Plane. NASA TN D-6788, 1972.

2. Roper, Alan T.; and Gentry, Garl L., Jr.: Turbulent-Boundary-Layer Development on a Moving Ground Belt of Rough Texture. NASA TM X2515, 1972.

3. Roper, Alan T.; and Gentry, Garl L., Jr.: Growth of Turbulent Boundary Layers over Nonstationary Boundaries. AIAA Journal, vol. 12, no. 1, Jan. 1974, pp 95-96.

4. Schlichting, H.: Lecture Series "Boundary Layer Theory". Part II - Turbulent Flows. NACA TM-1218, 1949.

5. Mirels, Harold: Boundary Layer Behind Shock or Thin Expansion Wave Moving Into Stationary Fluid. NACA TN-3712, 1956.

6. Clauser, Francis H.: Turbulent Boundary Layers in Adverse Pressure Gradients. J. Aeronaut. Sci., vol. 21, no. 2, Feb. 19554, pp 91-108.

TABLE I.- SUMMARY OF MULTIPLE DATA POINT MEASUREMENTS

x (m)	10 Data Point Measurements $R = V_B/U$	30 Data Point Measurements $R = V_B/U$
1.37	None	0, 0.245, 0.491, 0.739
2.61	0, 0.243, 0.487	-, -, -, 0.737
3.34	0, 0.242, -	-, -, 0.492, 0.740
4.26	0, 0.242, 0.486	None
5.17	-, 0.242, 0.484	0, -, -, 0.685

TABLE II.- DATA FROM BOUNDARY-LAYER SURVEYS

(a) x = 1.37m (4.50 ft)

R = 0.00 δ = 2.908 cm (1.145 in.)		R = 0.245 δ = 2.474 cm (0.974 in.)		R = 0.491 δ = 2.136 cm (0.841 in.)		R = 0.739 δ = 2.700 cm (1.063 in.)	
y/δ	u/U	y/δ	u/U	y/δ	u/U	y/δ	u/U
0.0961	0.6256	0.1129	0.6824	0.1308	0.7920	0.1035	0.8814
0.1659	0.7019	0.1950	0.7536	0.2259	0.8480	0.1788	0.9076
0.2096	0.7313	0.2464	0.7914	0.2853	0.8599	0.2258	0.9104
0.2707	0.7566	0.3182	0.8116	0.3685	0.8881	0.2916	0.9229
0.3231	0.7770	0.3798	0.8392	0.4398	0.9075	0.3481	0.9309
0.3580	0.7981	0.4209	0.8489	0.8474	0.9130	0.3857	0.9384
0.4104	0.8205	0.4824	0.8664	0.5587	0.9288	0.4422	0.9497
0.4628	0.8501	0.5440	0.9029	0.6300	0.9528	0.4986	0.9583
0.5065	0.8738	0.5954	0.9251	0.6895	0.9633	0.5457	0.9712
0.5589	0.8942	0.6569	0.9290	0.7608	0.9686	0.6021	0.9744
0.6026	0.8931	0.7083	0.9425	0.8202	0.9798	0.6492	0.9804
0.6637	0.9308	0.7801	0.9646	0.9034	0.9902	0.7150	0.9840
0.7161	0.9397	0.8417	0.9713	0.9750	0.9952	0.7714	0.9959
0.7859	0.9603	0.9238	0.9852	1.0702	0.9999	0.8467	0.9939
0.8383	0.9689	0.9856	0.9911			0.9031	0.9970
0.8995	0.9822	1.0575	0.9965			0.9690	1.0010
0.9782	0.9978	1.1499	0.9992			1.0536	1.0024
1.0480	1.0004						

TABLE II.- DATA FROM BOUNDARY-LAYER SURVEYS (CONT.)

(b) x = 2.62 m (8.58 ft)

R = 0.00 δ = 4.884 cm (1.924 in.)		R = 0.243 δ = 3.471 cm (1.406 in.)		R = 0.487 δ = 3.129 cm (1.232 in.)		R = 0.737 δ = 3.818 cm (1.503 in.)	
y/δ	u/U	y/δ	u/U	y/δ	u/U	y/δ	u/U
0.0884	0.5959	0.1210	0.6914	0.1379	0.8294	0.0865	0.8877
0.1300	0.6515	0.1779	0.7502	0.2029	0.8585	0.1331	0.9046
0.1663	0.6771	0.2277	0.7776	0.2521	0.8745	0.1730	0.9127
0.1871	0.7056	0.2561	0.8015	0.2921	0.8941	0.2195	0.9151
0.2235	0.7208	0.3059	0.8216	0.3489	0.9044	0.2528	0.9254
0.2243	0.7362	0.3344	0.8348	0.3814	0.9075	0.2794	0.9293
0.2807	0.7543	0.3842	0.8562	0.4382	0.9248	0.3127	0.9373
0.3223	0.7814	0.4411	0.8632	0.5031	0.9361	0.3659	0.9460
0.3743	0.8164	0.5123	0.8918	0.5843	0.9524	0.3925	0.9542
0.4107	0.8174	0.5621	0.9119	0.6411	0.9623	0.4324	0.9610
0.4418	0.8422	0.6048	0.9170	0.6897	0.9702	0.4790	0.9642
0.4782	0.8488	0.6546	0.9352	0.7465	0.9782	0.5123	0.9675
0.5094	0.8649	0.6973	0.9488	0.7952	0.9801	0.5522	0.9745
0.5510	0.8740	0.7542	0.9555	0.8601	0.9848	0.6121	0.9752
0.5822	0.8825	0.7969	0.9515	0.9088	0.9794	0.6520	0.9856
0.6186	0.9074	0.8467	0.9703	0.9657	0.9962	0.7119	0.9789
0.6602	0.9199	0.9036	0.9810	1.0305	0.9966	0.7584	0.9924
0.6966	0.9305	0.9534	0.9877			0.8117	0.9910
0.7589	0.9447	1.0388	0.9961			0.8782	0.9951
0.7953	0.9573					0.9181	0.9945
0.8681	0.9734					1.0112	0.9964
0.9253	0.9826						
0.9980	0.9914						
1.0656	0.9967						

TABLE II.- DATA FROM BOUNDARY-LAYER SURVEYS (CONT.)

(c) $\bar{x}$ = 3.35 m (11.00 ft)

R = 0.00 δ = 5.794 cm (2.281 in.)		R = 0.242 δ = 4.808 cm (1.893 in.)		R = 0.492 δ = 4.338 cm (1.708 in.)		R = 0.740 δ = 4.333 cm (1.706 in.)	
y/δ	u/U	y/δ	u/U	y/δ	u/U	y/δ	u/U
0.0526	0.4749	0.0634	0.6946	0.0761	0.7830	0.0762	0.8859
0.0833	0.5952	0.1004	0.7324	0.1171	0.8015	0.1172	0.8979
0.1140	0.6316	0.1373	0.7542	0.1406	0.8147	0.1407	0.9049
0.1403	0.6678	0.1690	0.7756	0.1757	0.8319	0.1759	0.9070
0.1622	0.6910	0.1954	0.7900	0.2050	0.8446	0.2052	0.9233
0.1841	0.6929	0.2219	0.8019	0.2284	0.8462	0.2286	0.9228
0.2148	0.7129	0.2588	0.8157	0.2577	0.8641	0.2579	0.9296
0.2411	0.7316	0.2905	0.8329	0.3045	0.8829	0.3048	0.9362
0.2894	0.7603	0.3486	0.8574	0.3631	0.8976	0.3634	0.9512
0.3244	0.7694	0.3909	0.8740	0.3982	0.9129	0.3986	0.9526
0.3507	0.7925	0.4226	0.8934	0.4451	0.9235	0.4455	0.9583
0.3770	0.8019	0.4543	0.8868	0.4744	0.9163	0.4748	0.9637
0.4077	0.8190	0.4913	0.9016	0.5154	0.9331	0.5158	0.9656
0.4384	0.8389	0.5282	0.9205	0.5681	0.9398	0.5686	0.9724
0.4691	0.8340	0.5652	0.9138	0.5974	0.9513	0.5979	0.9758
0.4998	0.8570	0.6022	0.9335	0.6442	0.9556	0.6448	0.9822
0.5349	0.8672	0.6445	0.9510	0.6911	0.9736	0.6917	0.9876
0.5612	0.8793	0.6761	0.9553	0.7379	0.9742	0.7386	0.9885
0.6182	0.8941	0.7448	0.9701	0.7965	0.9843	0.7972	0.9862
0.6489	0.9114	0.7818	0.9702	0.8433	0.9816	0.8441	0.9897
0.7015	0.9266	0.8452	0.9818	0.9136	0.9904	0.9144	0.9924
0.7628	0.9393	0.9878	0.9911	0.9898	0.9855	0.9906	0.9914
0.8198	0.9618	1.0565	0.9939	1.0659	0.9920	1.0668	0.9933
0.9864	0.9867	1.1146	0.9971				
1.0303	0.9875						
1.0829	0.9903						
1.1179	0.9934						

TABLE II.- DATA FROM BOUNDARY-LAYER SURVEYS (CONT.)

(d) x = 4.27 m (14.00 ft)

R = 0.000
δ = 8.230 cm (3.240 in.)

y/δ	u/U
0.0340	0.5593
0.0525	0.6083
0.0679	0.6369
0.0833	0.6520
0.0988	0.6647
0.1141	0.6845
0.1296	0.6967
0.1482	0.7040
0.1605	0.7221
0.1852	0.7366
0.2037	0.7551
0.2191	0.7619
0.2438	0.7756
0.2654	0.7838
0.2840	0.7899
0.3087	0.8046
0.3334	0.8177
0.3550	0.8276
0.3920	0.8483
0.4136	0.8532
0.4537	0.8734
0.4939	0.8821
0.5340	0.8989
0.5741	0.9112
0.6112	0.9255
0.6513	0.9371
0.6852	0.9424
0.7192	0.9542
0.7346	0.9466
0.7809	0.9731
0.8272	0.9807
0.8519	0.9789
0.8982	0.9904
0.9322	0.9902
0.9723	0.9899
1.0093	0.9876

R = 0.242
δ = 6.073 cm (2.391 in.)

y/δ	u/U
0.0460	0.6855
0.0711	0.7223
0.0920	0.7396
0.1129	0.7549
0.1338	0.7723
0.1505	0.7776
0.1756	0.7917
0.2007	0.8082
0.2174	0.8210
0.2509	0.8281
0.2760	0.8428
0.2969	0.8446
0.3304	0.8628
0.3596	0.8719
0.3847	0.8740
0.4182	0.8971
0.4516	0.9040
0.4809	0.9170
0.5311	0.9232
0.5603	0.9327
0.6147	0.9479
0.6691	0.9576
0.7234	0.9593
0.7778	0.9777
0.8280	0.9851
0.8823	0.9917
0.9283	0.9904
0.9743	0.9924
0.9952	0.9885
1.0580	0.9966

R = 0.486
δ = 4.641 cm (1.827 in.)

y/δ	u/U
0.0602	0.7936
0.0931	0.8123
0.1204	0.8263
0.1478	0.8503
0.1752	0.8599
0.1971	0.8581
0.2299	0.8755
0.2628	0.8849
0.2847	0.8983
0.3285	0.9114
0.3613	0.9162
0.3887	0.9204
0.4325	0.9296
0.4708	0.9356
0.5036	0.9320
0.5474	0.9512
0.5912	0.9619
0.6296	0.9655
0.6953	0.9714
0.7336	0.9755
0.8047	0.9833
0.8759	0.9875
0.9471	0.9907
1.0182	0.9228

TABLE II.- DATA FROM BOUNDARY-LAYER SURVEYS (CONCLUDED)

(e) x = 5.18 m (17.00 ft)

R = 0.000 δ = 8.948 cm (3.523 in.)		R = 0.242 δ = 7.120 cm (2.803 in.)		R = 0.484 δ = 5.321 cm (2.095 in.)		R = 0.685 δ = 5.377 cm (2.117 in.)	
y/δ	u/U	y/δ	u/U	y/δ	u/U	y/δ	u/U
0.0341	0.4990	0.0392	0.6956	0.0525	0.8033	0.0567	0.8671
0.0539	0.5683	0.0607	0.7255	0.0811	0.8190	0.0898	0.8833
0.0681	0.6098	0.0821	0.7419	0.1098	0.8329	0.1134	0.8924
0.0795	0.6167	0.0999	0.7521	0.1336	0.8472	0.1323	0.8937
0.0937	0.6460	0.1177	0.7622	0.1575	0.8553	0.1559	0.9058
0.1192	0.6824	0.1320	0.7723	0.1766	0.8604	0.1748	0.9133
0.1703	0.7256	0.1534	0.7841	0.2052	0.8747	0.1984	0.9183
0.1873	0.7335	0.1748	0.8046	0.2338	0.8791	0.2362	0.9204
0.2072	0.7610	0.1962	0.8148	0.2625	0.8928	0.2834	0.9441
0.2242	0.7578	0.2141	0.8262	0.2863	0.8975	0.3118	0.9421
0.2413	0.7659	0.2391	0.8365	0.3198	0.9037	0.3449	0.9385
0.2640	0.7673	0.2605	0.8440	0.3484	0.9121	0.3732	0.9577
0.2839	0.7856	0.2819	0.8589	0.3770	0.9218	0.4015	0.9524
0.3037	0.7874	0.3104	0.8616	0.4152	0.9383	0.4393	0.9568
0.3264	0.7979	0.3318	0.8588	0.4438	0.9280	0.4724	0.9621
0.3548	0.8233	0.3604	0.8807	0.4820	0.9403	0.5055	0.9694
0.3804	0.8214	0.3925	0.8910	0.5250	0.9514	0.5433	0.9663
0.4002	0.8414	0.4139	0.8980	0.5536	0.9580	0.5905	0.9715
0.4371	0.8446	0.4567	0.9040	0.6109	0.9702	0.6330	0.9795
0.4712	0.8701	0.4817	0.9204	0.6443	0.9719	0.6661	0.9738
0.5053	0.8739	0.5281	0.9212	0.7063	0.9795	0.7275	0.9878
0.5422	0.8934	0.5780	0.9381	0.7731	0.9849	0.7842	0.9891
0.5762	0.8816	0.6173	0.9474	0.8256	0.9841	0.8408	0.9937
0.6131	0.9001	0.6672	0.9632	0.8926	0.9910	0.9022	0.9925
0.6784	0.9363	0.7064	0.9696	0.9451	0.9931	0.9589	0.9932
0.7068	0.9409	0.7528	0.9787	1.0072	0.9919	1.0203	0.9943
0.7352	0.9561	0.7921	0.9785				
0.7778	0.9671	0.8313	0.9823				
0.8033	0.9643	0.8492	0.9840				
0.8459	0.9687	0.9027	0.9896				
0.8771	0.9621	0.9562	0.9930				
0.9112	0.9776	0.9848	0.9936				
0.9481	0.9829	1.0347	0.9916				
0.9736	0.9831						
1.0304	0.9938						

TABLE III.- SUMMARY OF GROSS PARAMETERS FROM PROFILE MEASUREMENTS

X		R	U		R_{x_4}	δ		δ^*		θ		H	N
m	ft		m/sec	ft/sec	x 10	cm	in	cm	in	cm	in		
1.37	4.50	0.000	29.83	97.88	2.62	2.908	1.145	.472	.186	.236	.093	1.998	4.887
		0.245	29.82	97.83	2.62	2.474	.974	.363	.144	.226	.089	1.613	4.021
		0.491	29.82	97.84	2.62	2.136	.841	.203	.080	.145	.057	1.411	3.853
		0.739	29.77	97.67	2.61	2.700	1.063	.112	.044	.091	.036	1.203	3.472
2.62	8.58	0.000	30.11	98.79	4.90	4.877	1.924	.919	.362	.523	.206	1.754	4.662
		0.243	30.10	98.76	4.90	3.571	1.406	.561	.221	.358	.141	1.564	4.209
		0.487	30.12	98.81	4.90	3.129	1.232	.290	.114	.211	.083	1.376	4.886
		0.737	29.86	97.95	5.00	3.818	1.503	.208	.082	.185	.073	1.120	4.071
3.35	11.00	0.000	30.24	99.20	6.24	5.794	2.281	1.130	.445	.716	.282	1.576	4.500
		0.242	30.25	99.25	6.25	4.808	1.893	.635	.250	.455	.179	1.398	5.071
		0.492	29.79	97.75	6.40	4.338	1.708	.490	.193	.401	.158	1.221	4.267
		0.740	29.76	97.65	6.39	4.333	1.706	.297	.117	.272	.107	1.088	4.133
4.27	14.00	0.000	30.25	99.23	7.91	8.230	3.240	1.313	.517	.904	.356	1.449	5.727
		0.242	30.19	99.06	7.89	6.073	2.391	.767	.302	.577	.227	1.329	5.523
		0.486	30.18	99.02	7.89	4.641	1.827	.419	.165	.343	.135	1.220	5.205
5.18	17.00	0.000	32.10	105.32	9.21	8.948	3.523	1.529	.602	1.041	.410	1.469	5.235
		0.242	30.22	99.16	9.61	7.120	2.803	.843	.332	.643	.253	1.311	5.873
		0.484	30.30	99.41	9.63	5.321	2.095	.465	.183	.386	.152	1.202	5.610
		0.685	32.13	105.40	9.22	5.377	2.117	.330	.130	.297	.117	1.111	5.013

TABLE III.- SUMMARY OF GROSS PARAMETERS FROM PROFILE MEASUREMENTS (CONCLUDED)

X		ζ	θ		θ^*		Θ		H
m	ft		cm	in	cm	in	cm	in	
1.37	4.50	0.000	2.908	1.145	.472	.186	.236	.093	1.998
		0.245	2.421	.953	.450	.177	.267	.105	1.690
		0.491	2.050	.807	.330	.130	.206	.081	1.606
		0.739	2.441	.961	.320	.126	.178	.070	1.814
2.62	8.58	0.000	4.887	1.924	.919	.362	.523	.206	1.754
		0.243	3.500	1.378	.688	.271	.427	.168	1.609
		0.487	3.038	1.196	.462	.182	.318	.125	1.447
		0.737	3.449	1.358	.668	.263	.503	.198	1.330
3.35	11.00	0.000	5.794	2.281	1.130	.445	.716	.282	1.576
		0.242	4.669	1.838	.803	.316	.551	.217	1.454
		0.492	4.094	1.612	.884	.348	.660	.260	1.335
		0.740	3.988	1.570	1.019	.401	.820	.323	1.243
4.27	14.00	0.000	8.230	3.240	1.313	.517	.904	.356	1.449
		0.242	5.865	2.309	.876	.345	.706	.278	1.333
		0.486	4.379	1.724	.749	.295	.564	.222	1.325
5.18	17.00	0.000	8.948	3.523	1.529	.602	1.041	.410	1.469
		0.242	6.922	2.725	1.080	.425	.790	.311	1.365
		0.484	5.027	1.979	.833	.328	.643	.253	1.297
		0.685	4.900	1.929	.940	.370	.747	.294	1.260

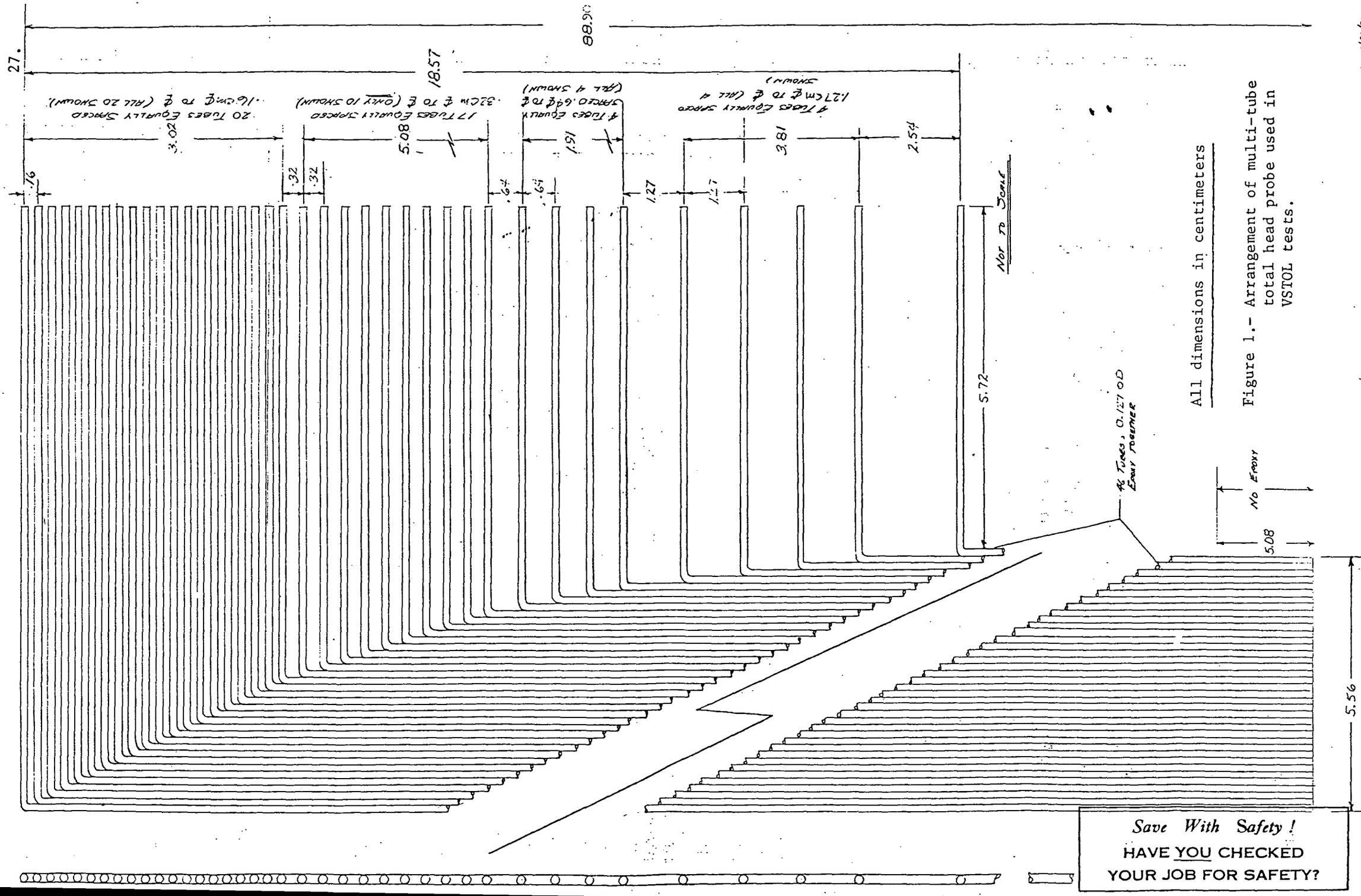

Figure 1.- Arrangement of multi-tube total head probe used in VSTOL tests.

Figure 1. - Velocity defect due to leading edge disturances.

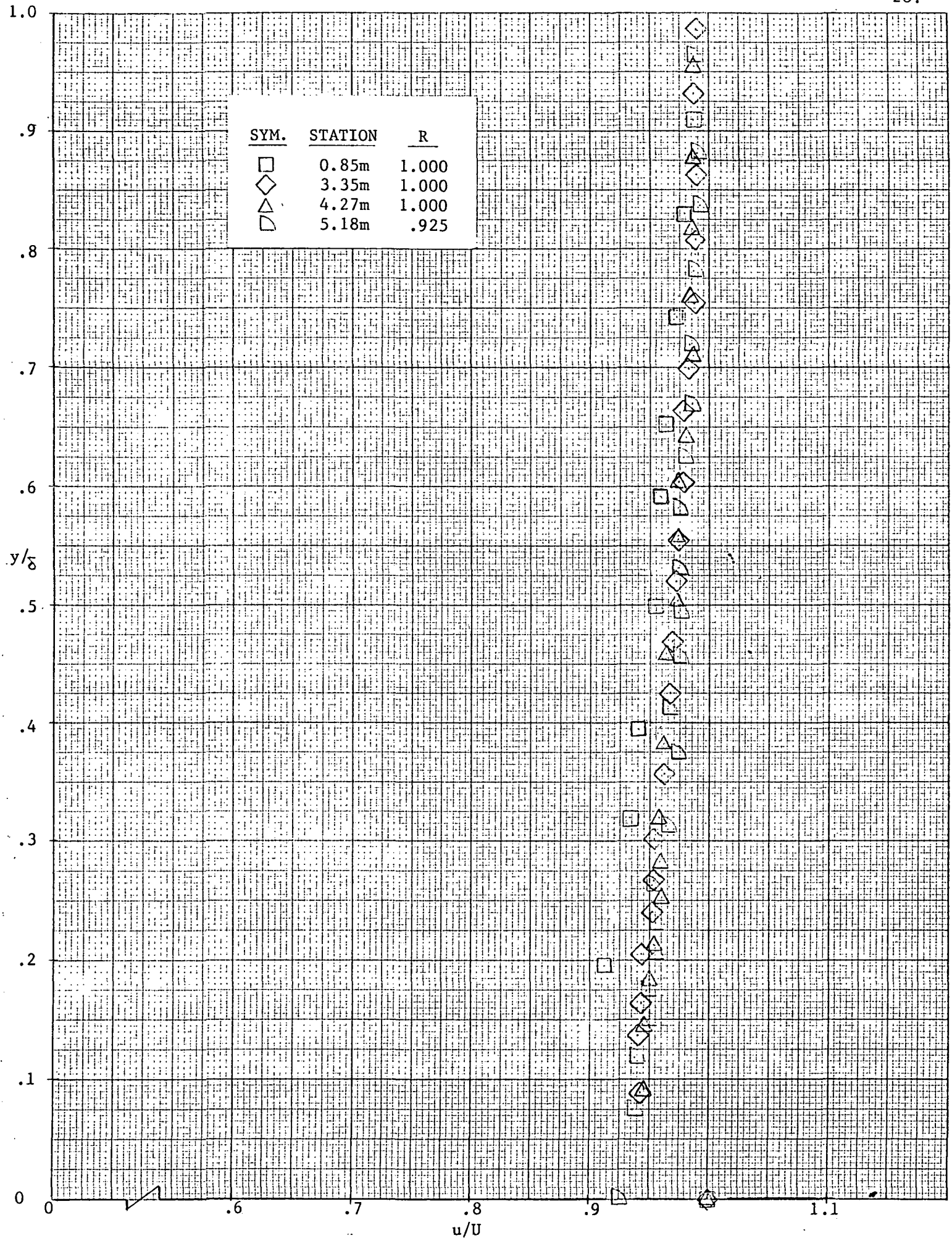

Figure 3(a).- Measured velocity profiles: Station x = 1.37m (4.50 ft)

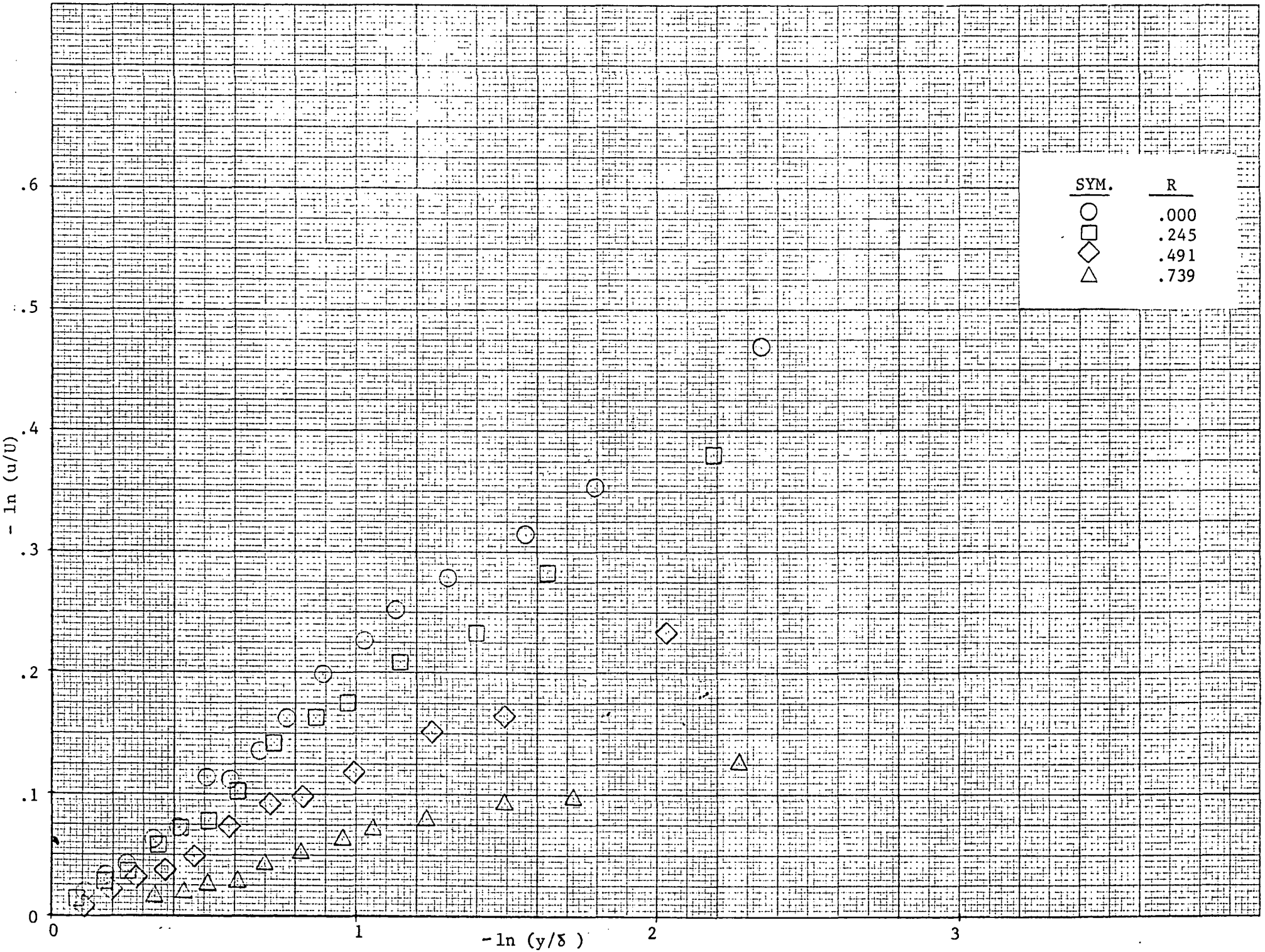

Figure 3(b).- Measured velocity profiles: Station x = 2.62m (8.58 ft): (continued)

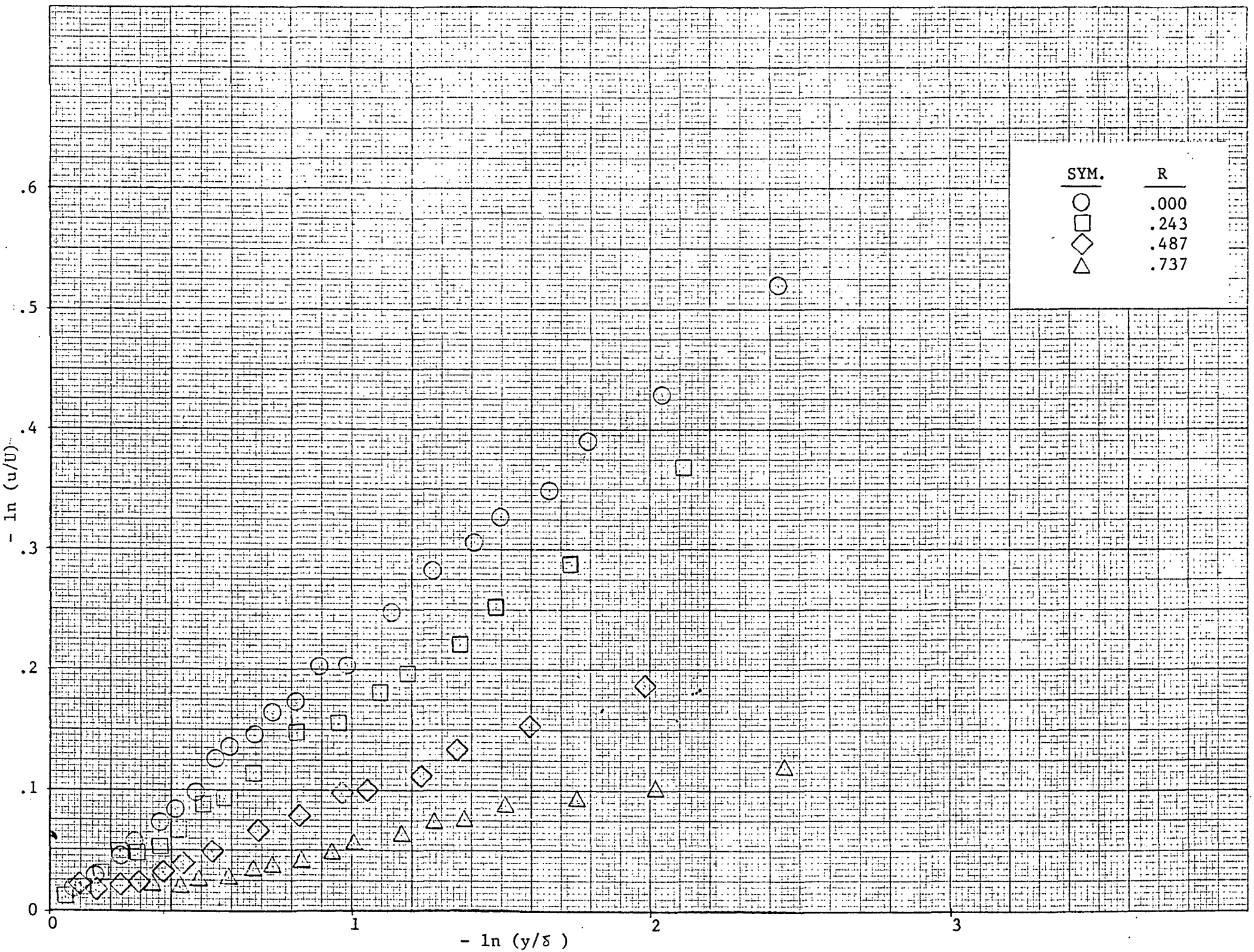

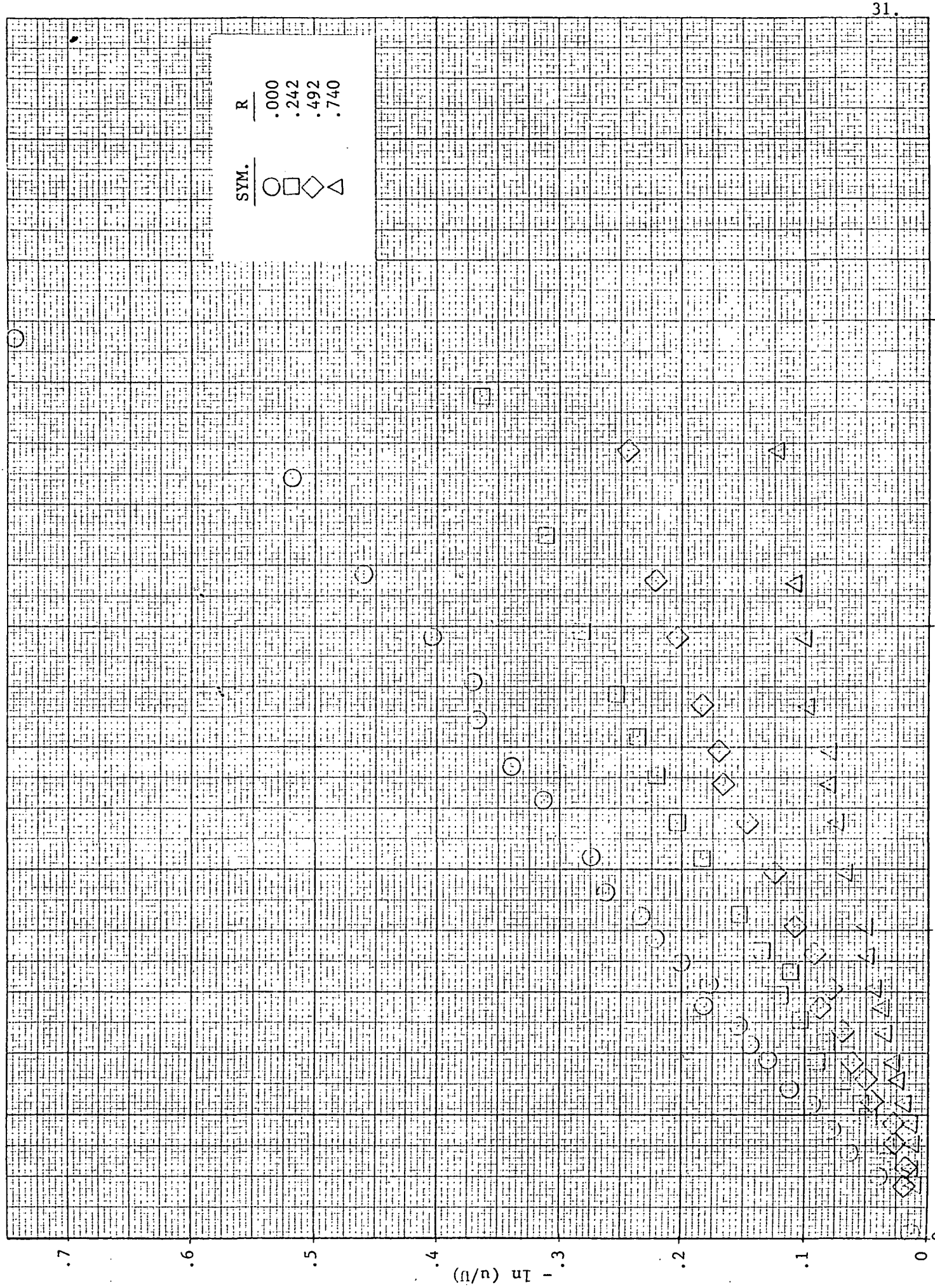

Figure 3(c).- Measured velocity profiles: Station x = 3.35m (11.00 ft): (continued)

Figure 3(d).- Measured velocity profiles: Station x = 4.27m (14.00 ft): (continued)

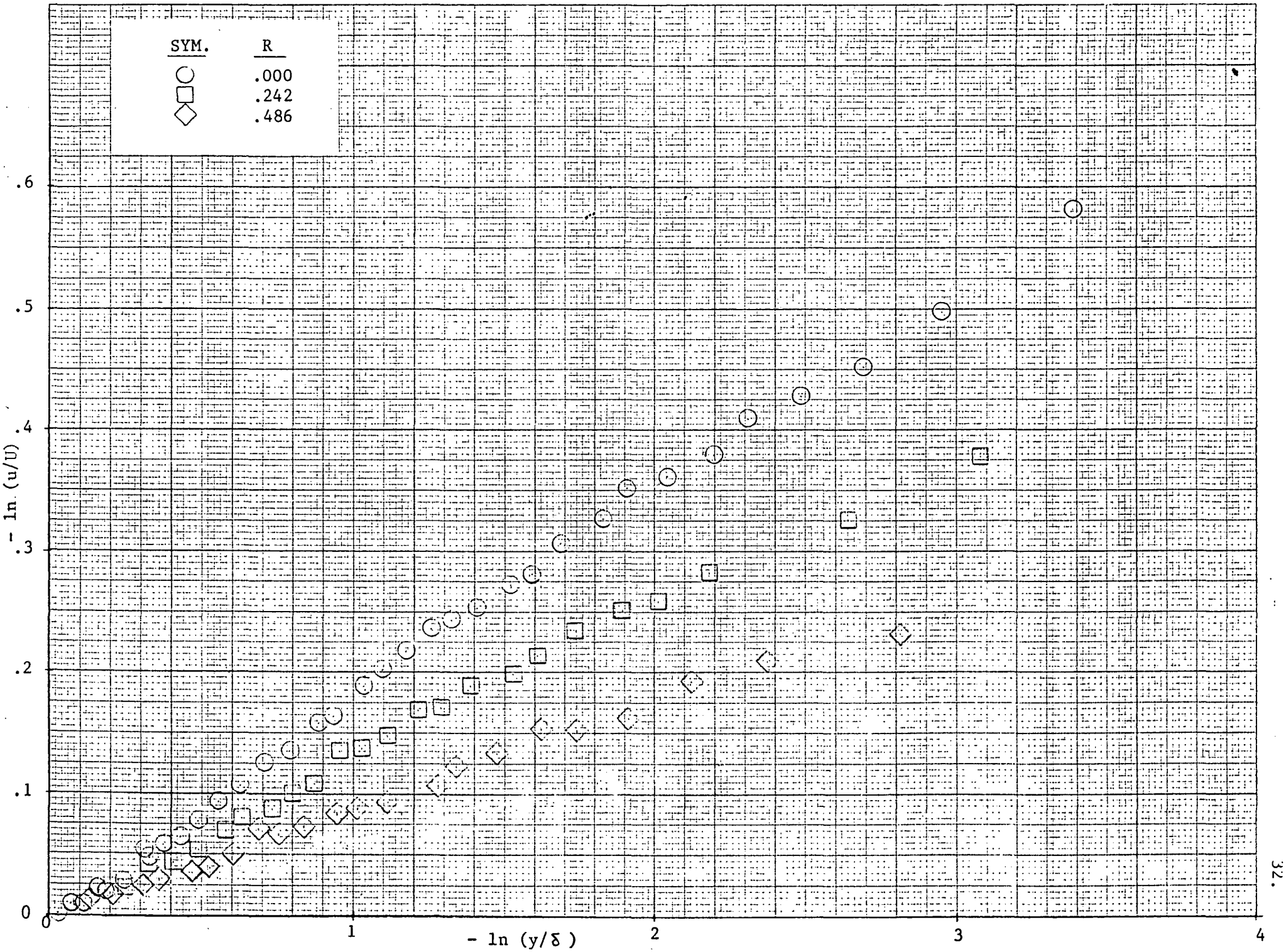

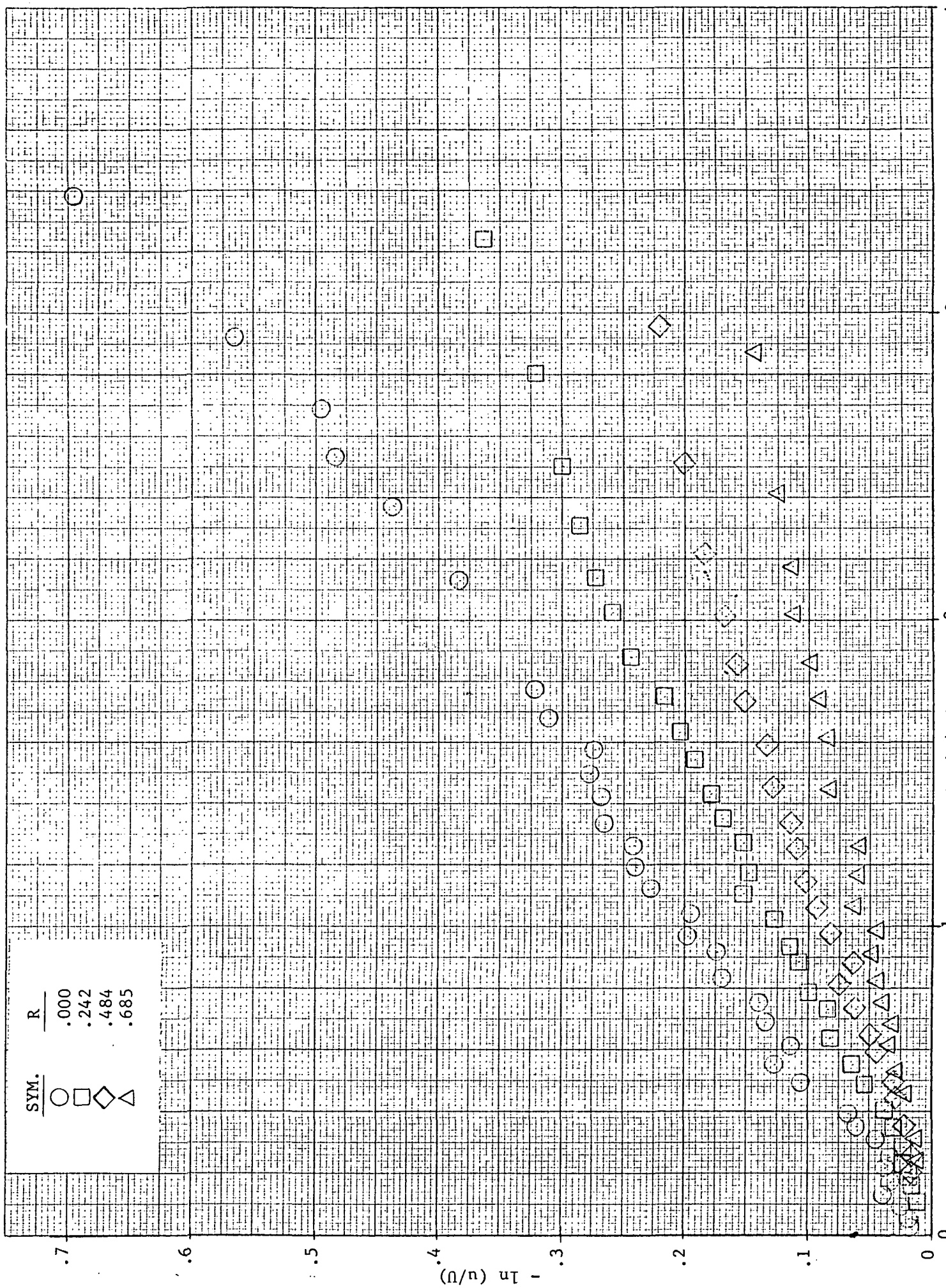

Figure 3(e).- Measured velocity profiles: Station x = 5.18m (17.00 ft): (concluded)

Figure 4.- Variation of boundary-layer thickness with ground-plane speed

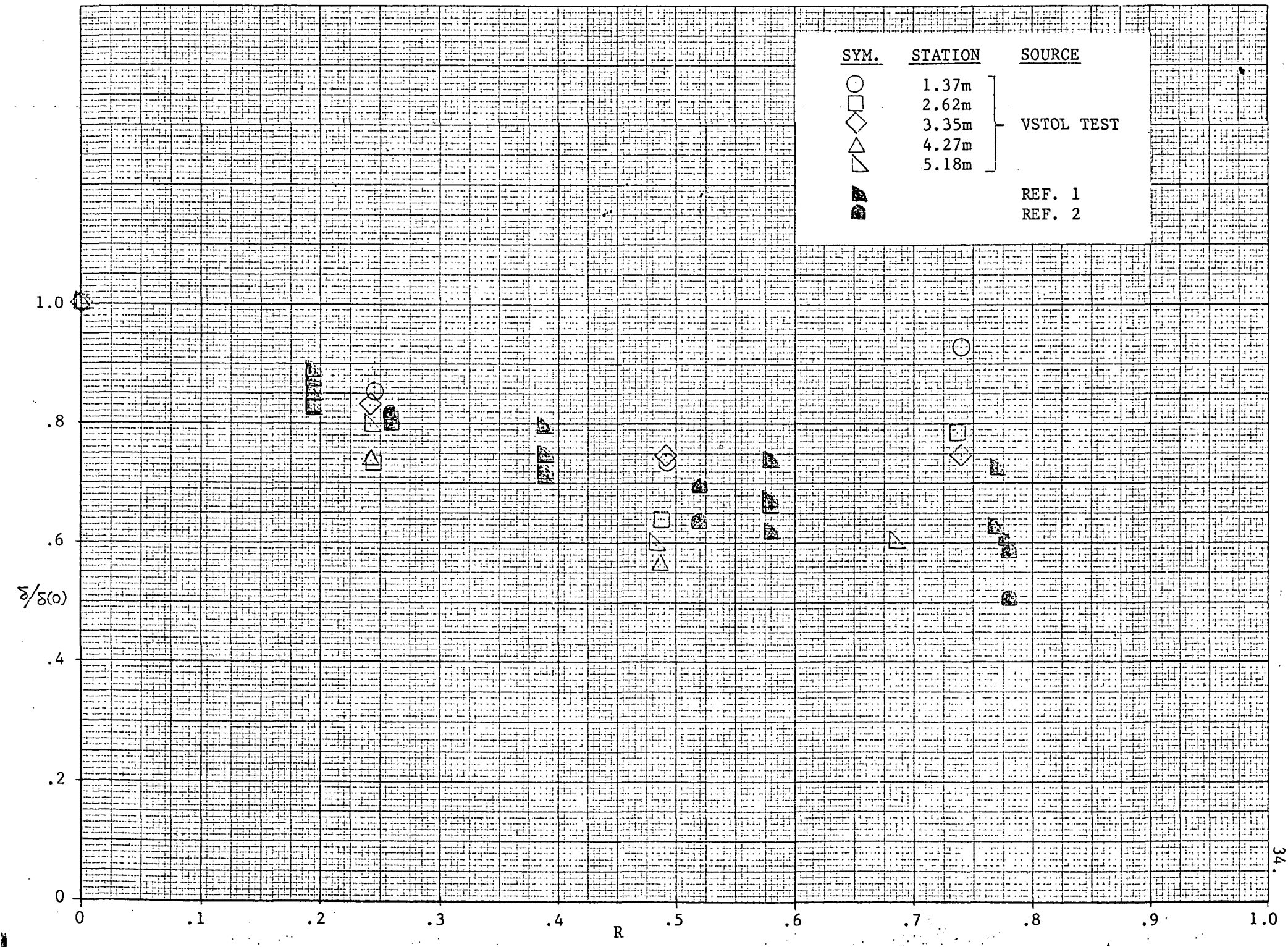

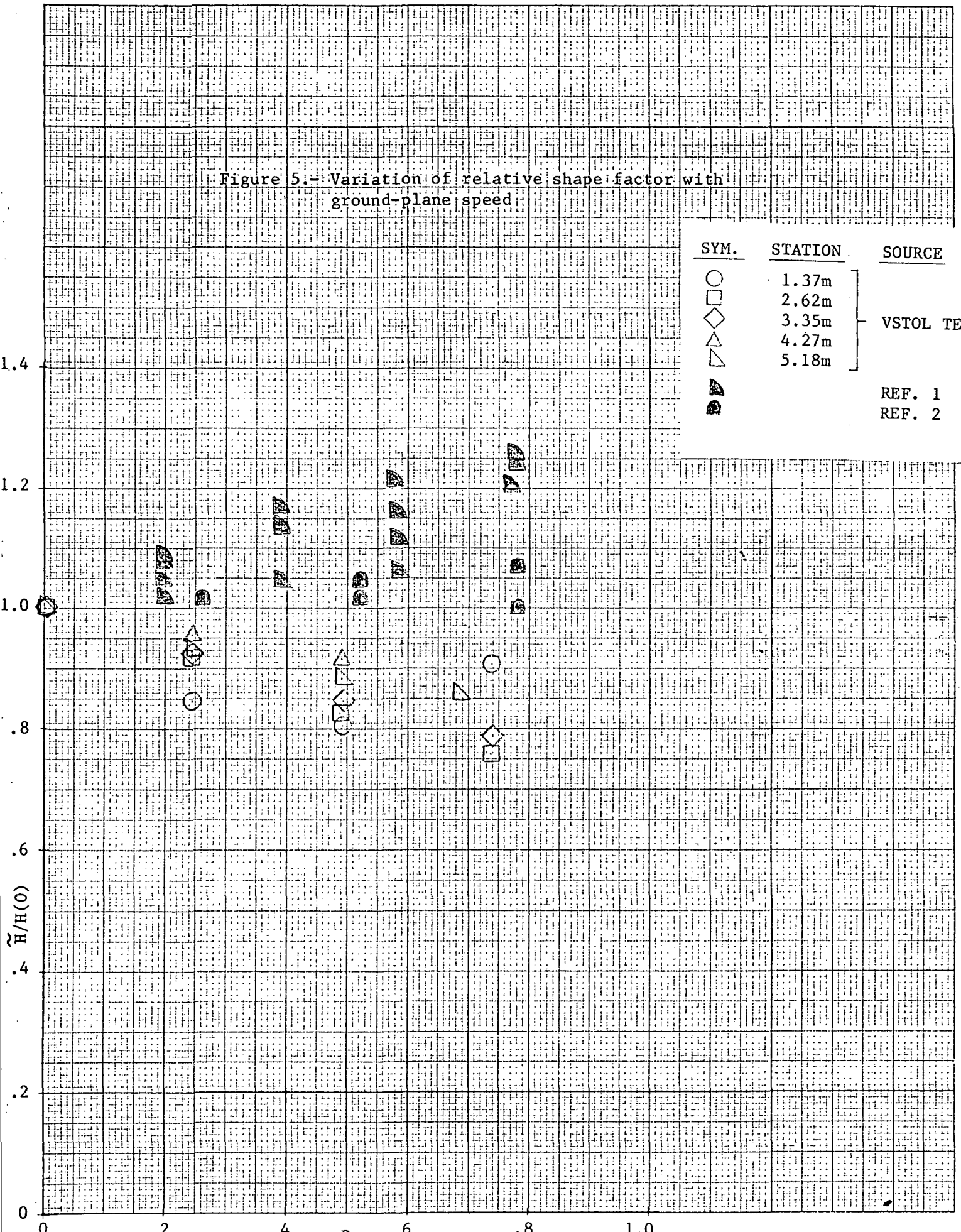

Figure 5.- Variation of relative shape factor with ground-plane speed

Figure 6.- Variation of $g(R) = \theta/\theta(0)$ with ground-plane speed

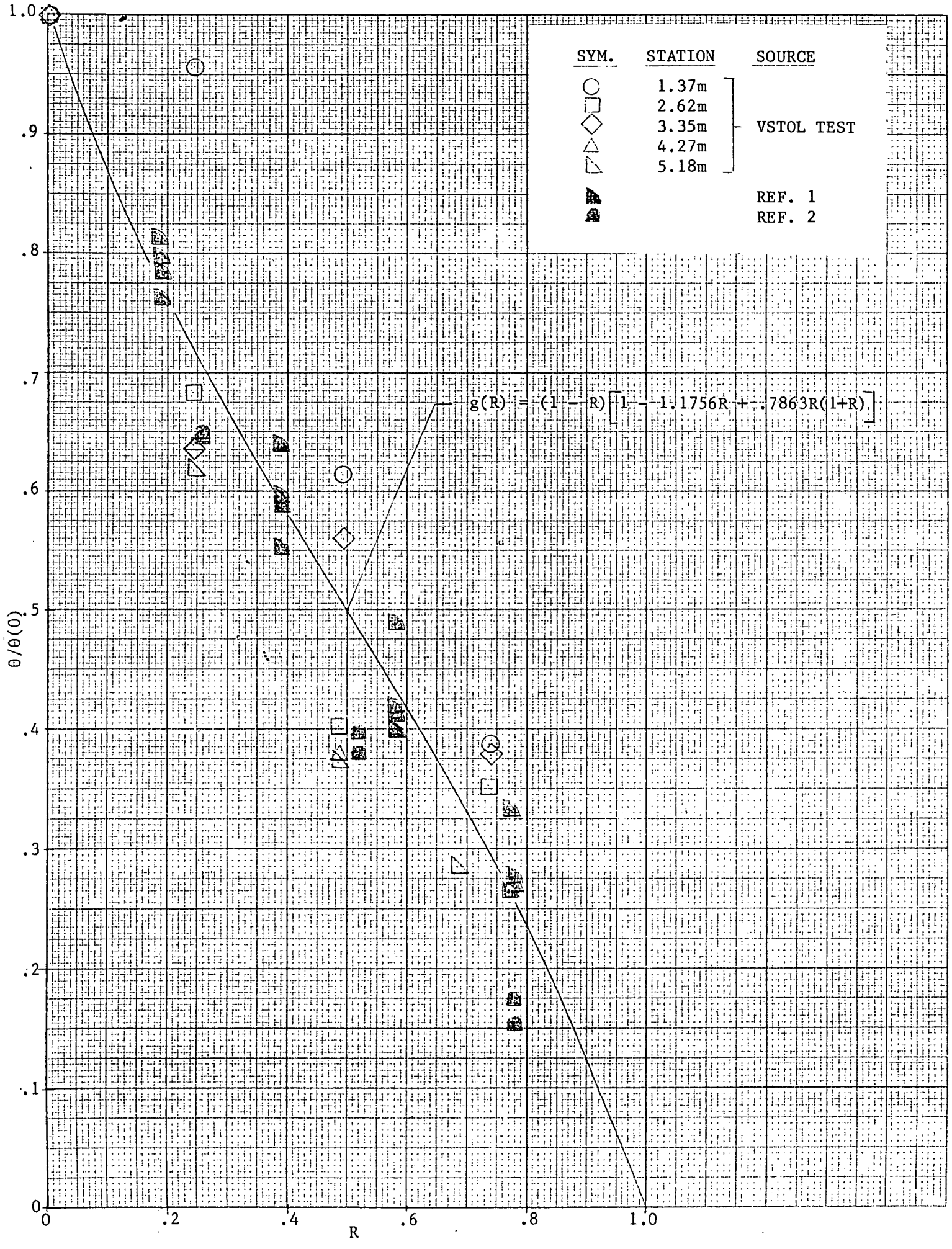

Figure 7(a).- Comparison of measured and predicted values of the integral parameters: Station 1.37m (4.50 ft)

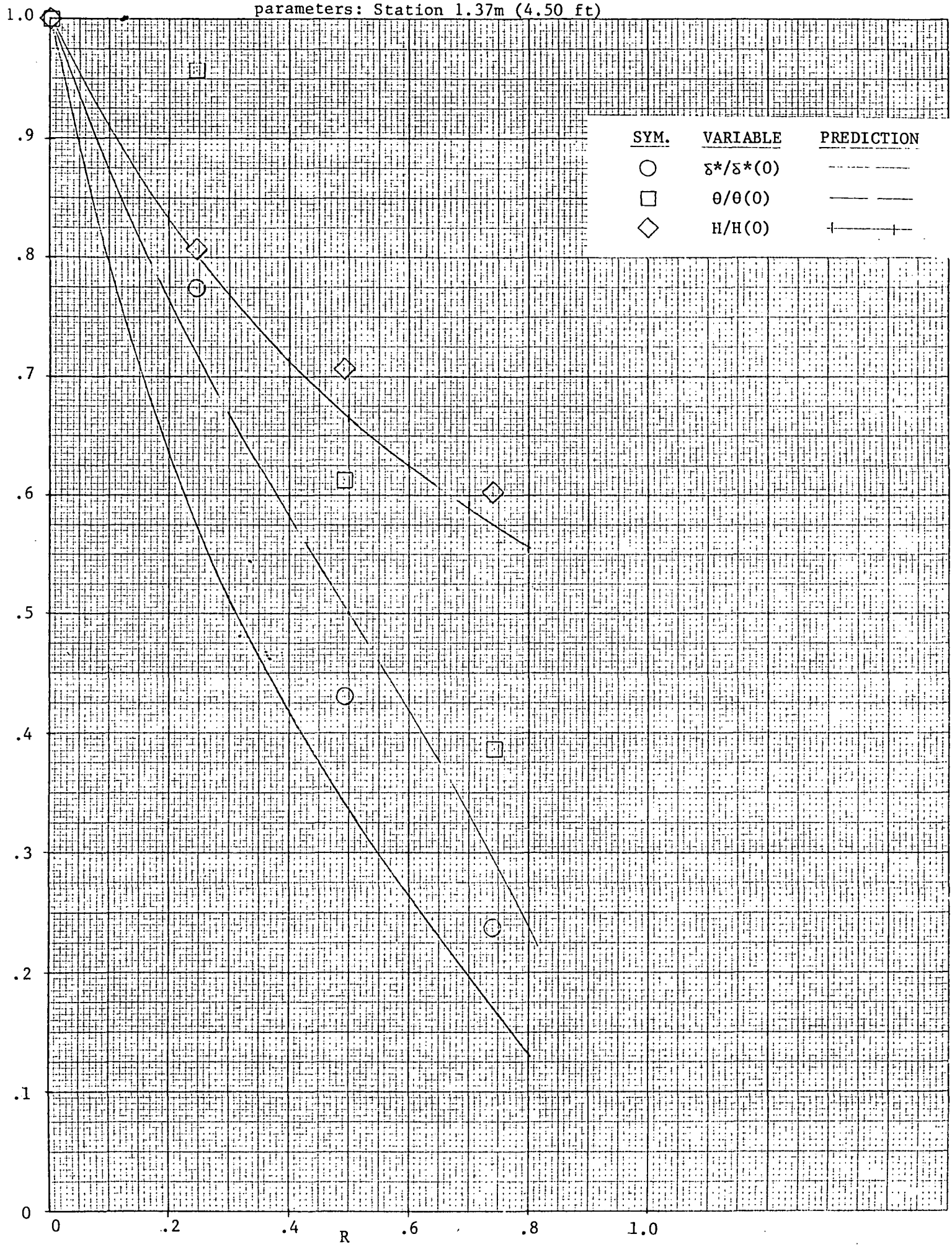

Figure 7(b).- Comparison of measured and predicted values of the integral parameters: Station 2.62m (8.58 ft): (continued)

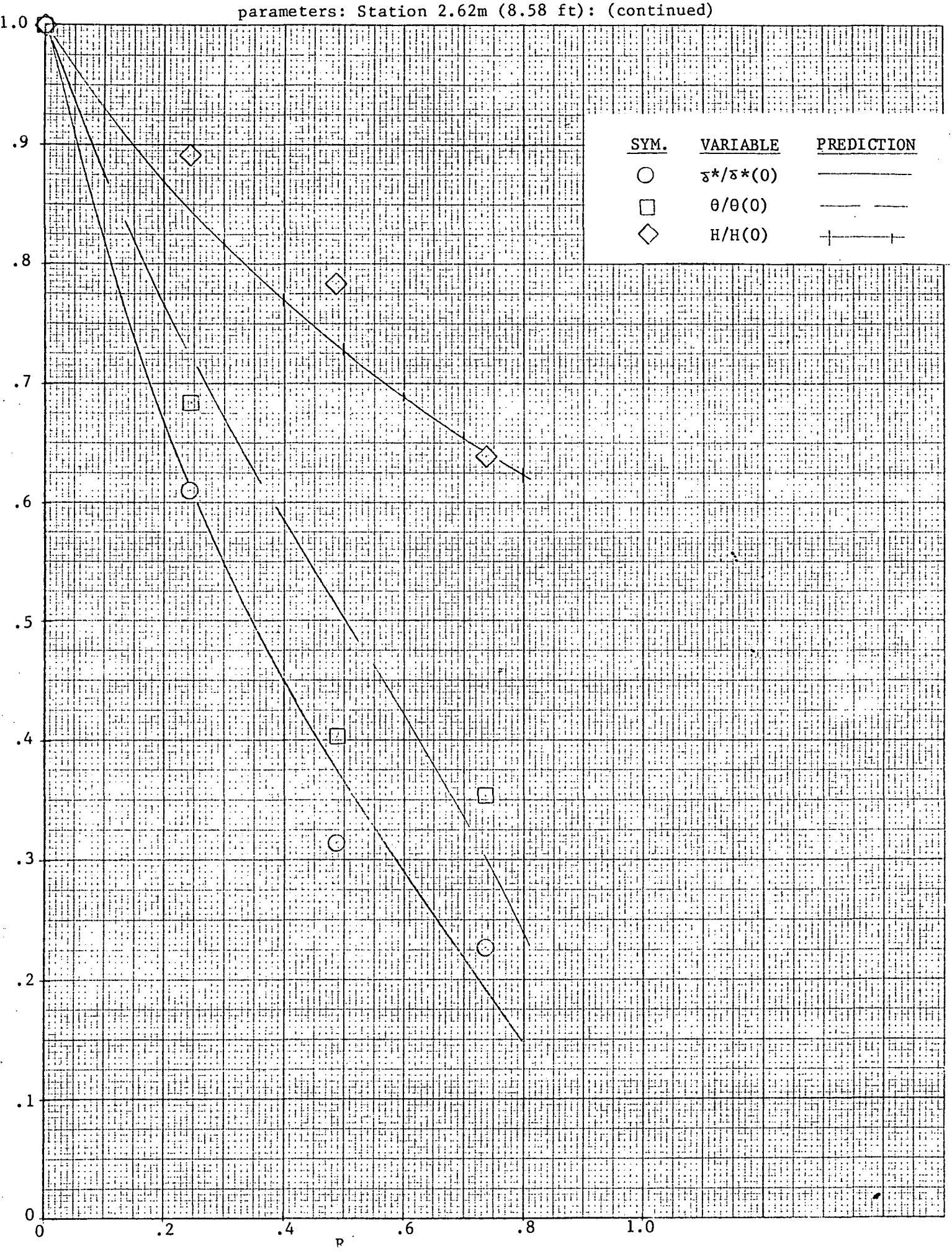

Figure 7(c).- Comparison of measured and predicted values of the integral parameters: Station 3.35m (11.00 ft): (continued)

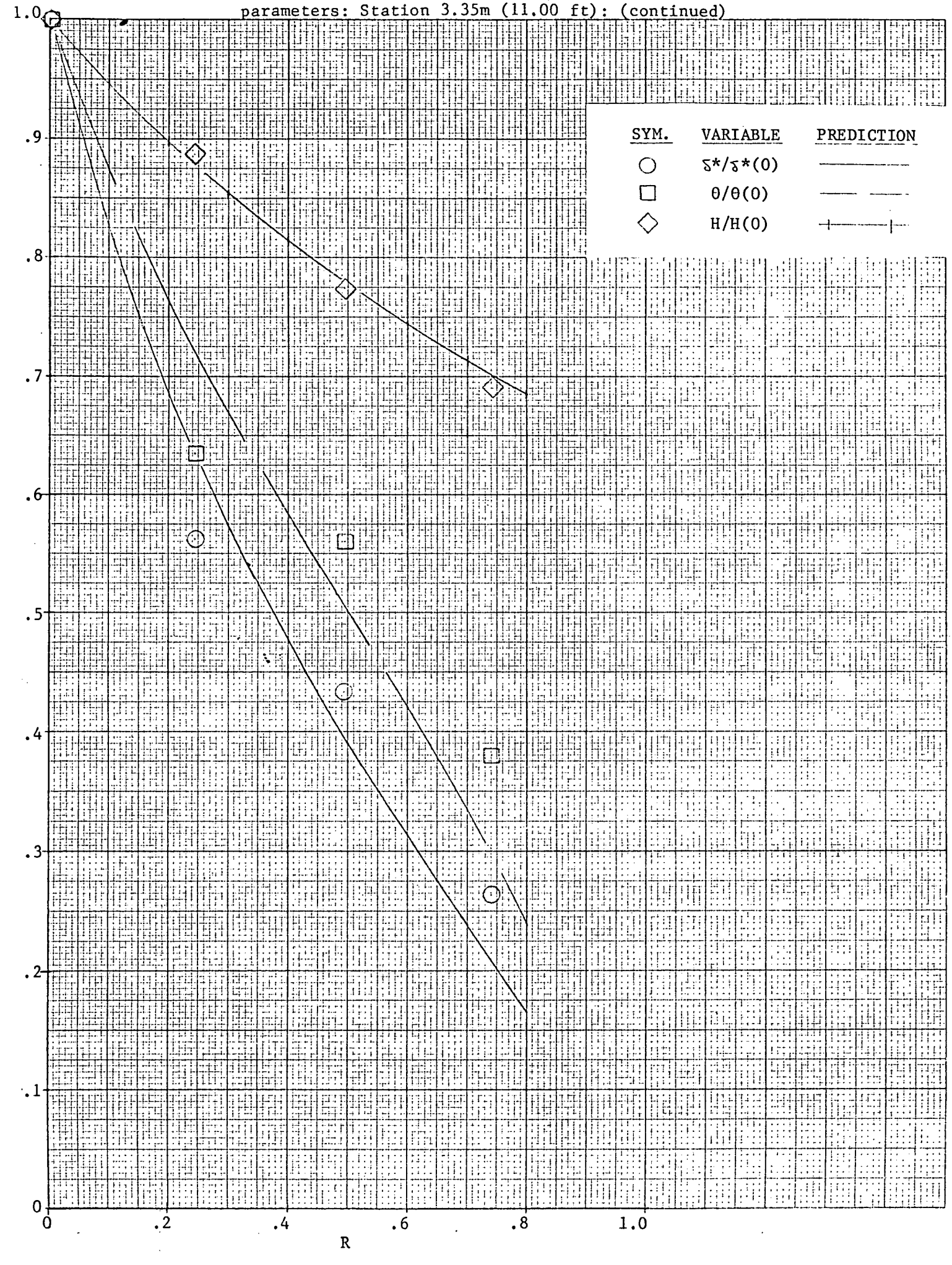

Figure 7(d).- Comparison of measured and predicted values of the integral parameters: Station 4.27m (14.00 ft): (continued)

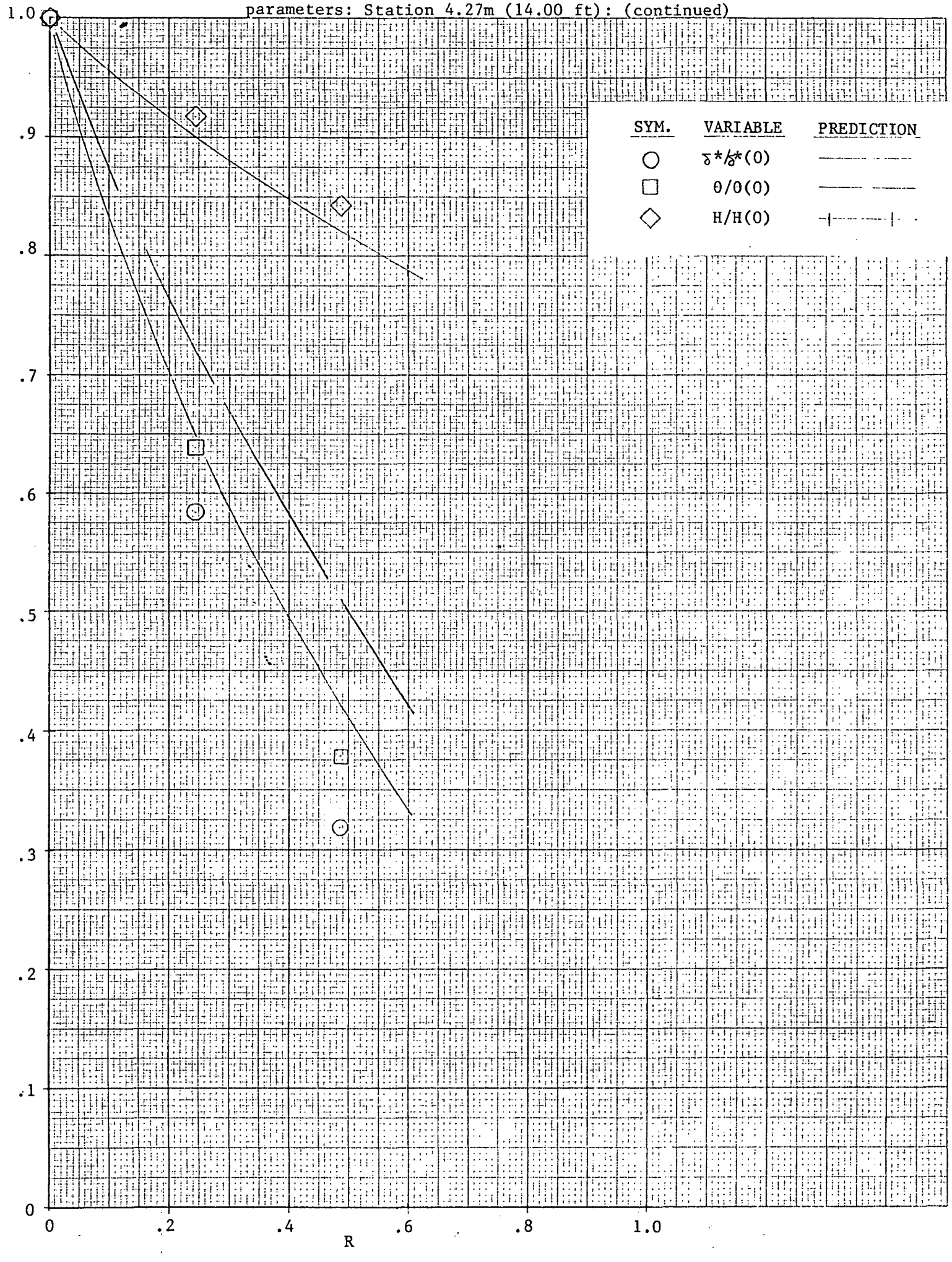

Figure 7(e).- Comparison of measured and predicted values of the integral parameters: Station 5.18m (17.00 ft): (concluded)

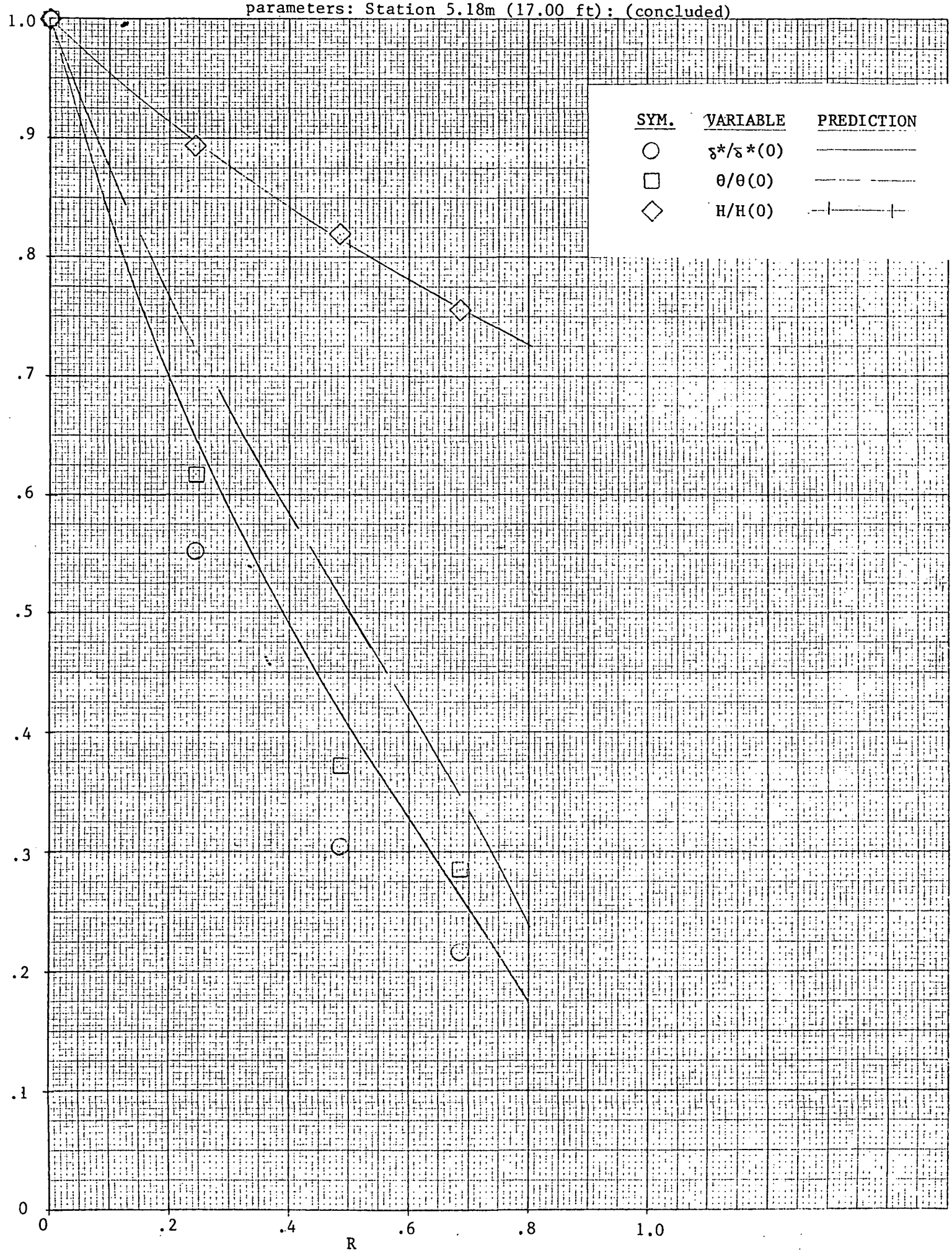

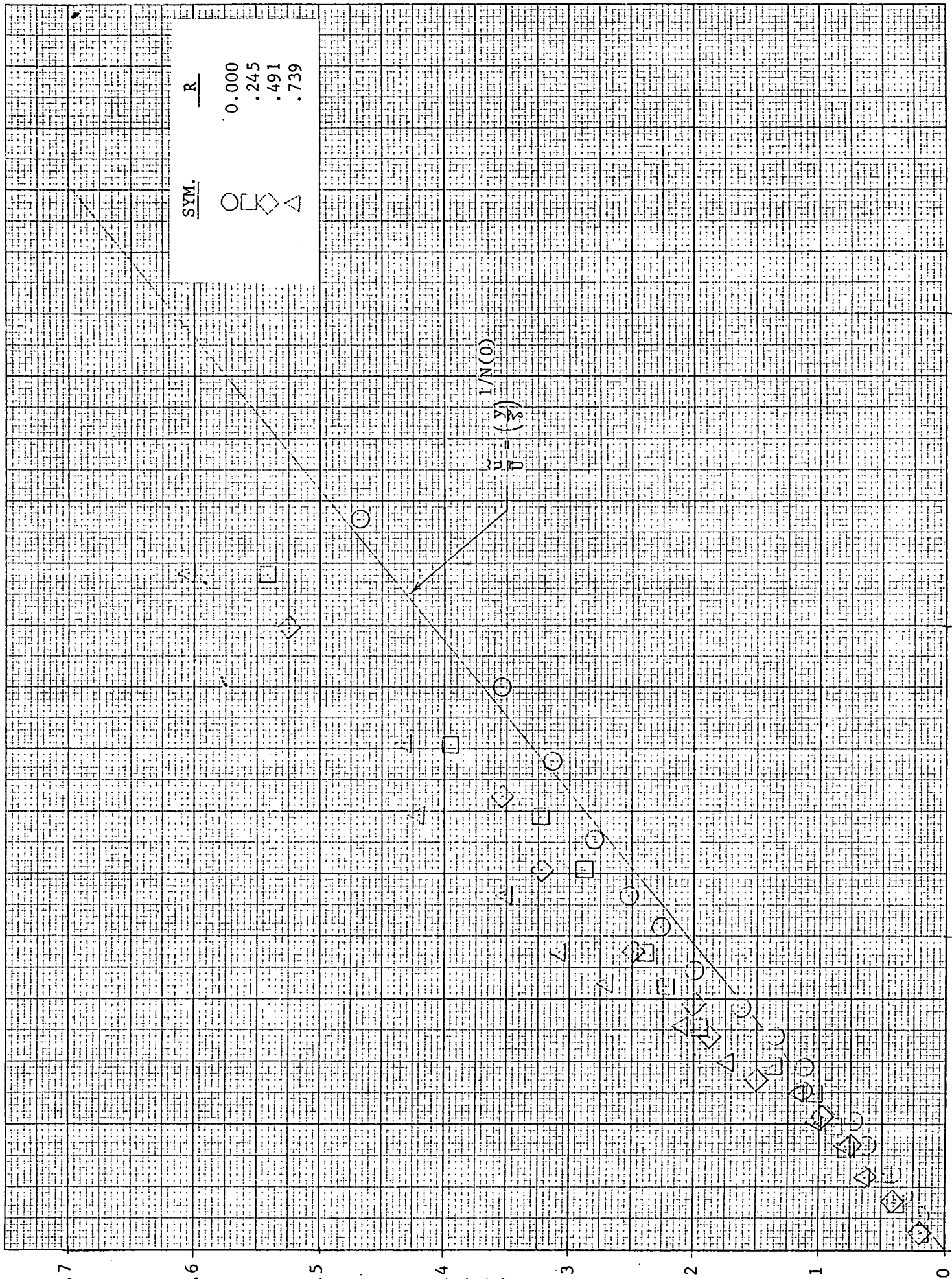

Figure 8(a).- Measured relative velocity profiles: Station x = 1.37m (4.50 ft)

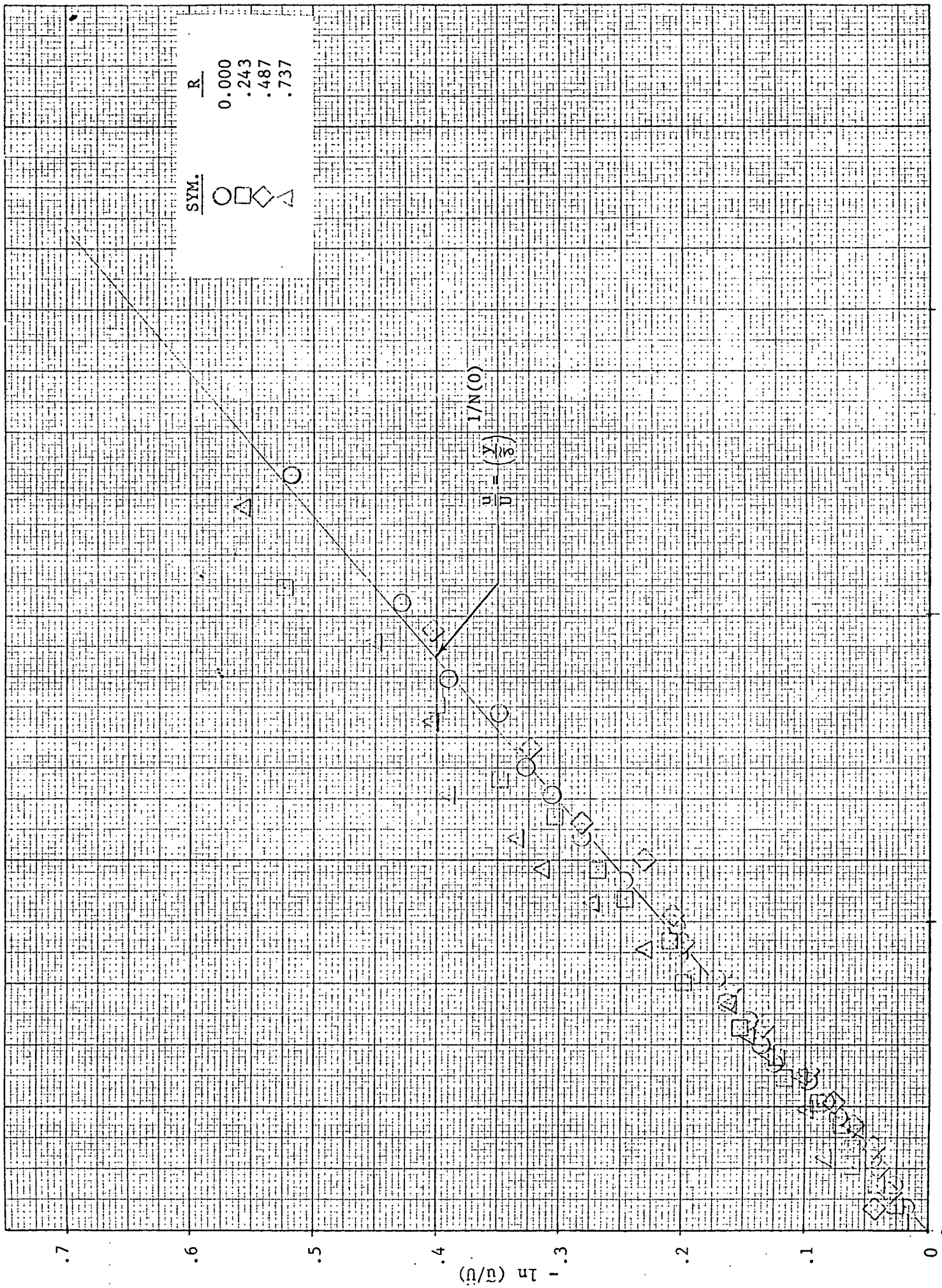

Figure 8(b).- Measured relative velocity profiles: Station x = 2.62m (8.58 ft): (continued)

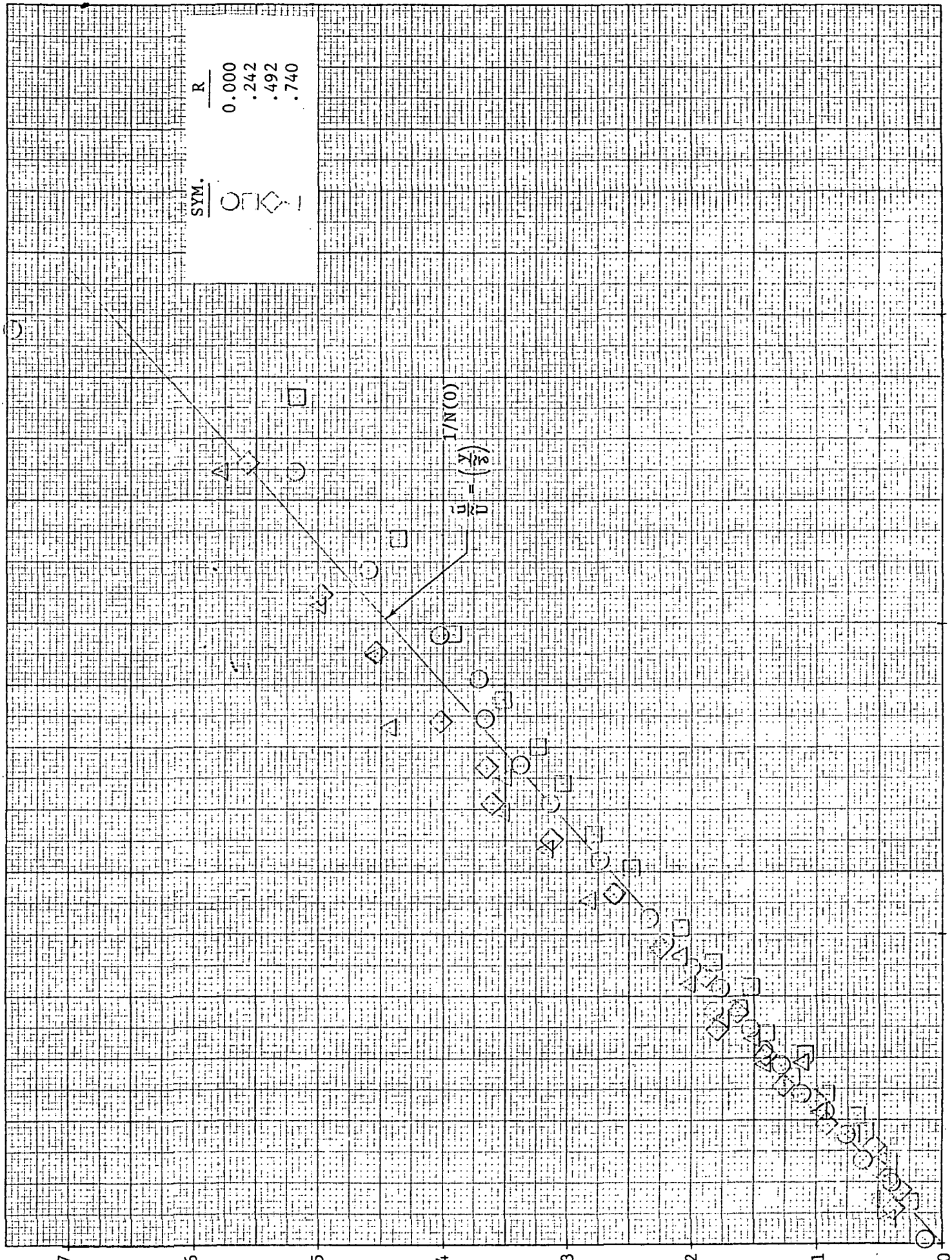

Figure 8(c).- Measured relative velocity profiles: Station x = 3.35m (11.00 ft): (continued)

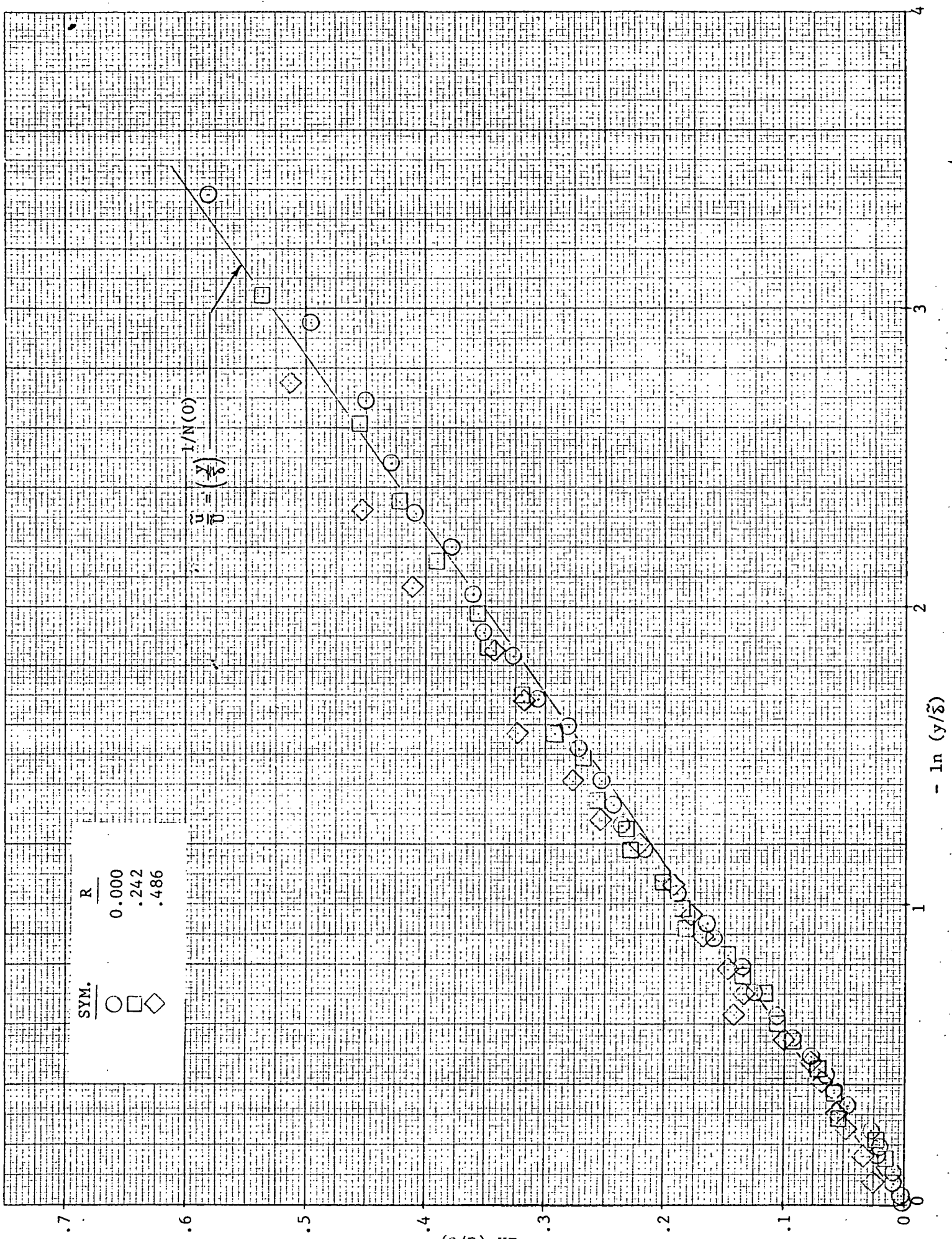

Figure 8(d).- Measured relative velocity profiles: Station x = 4.27m (14.00 ft): (continued)

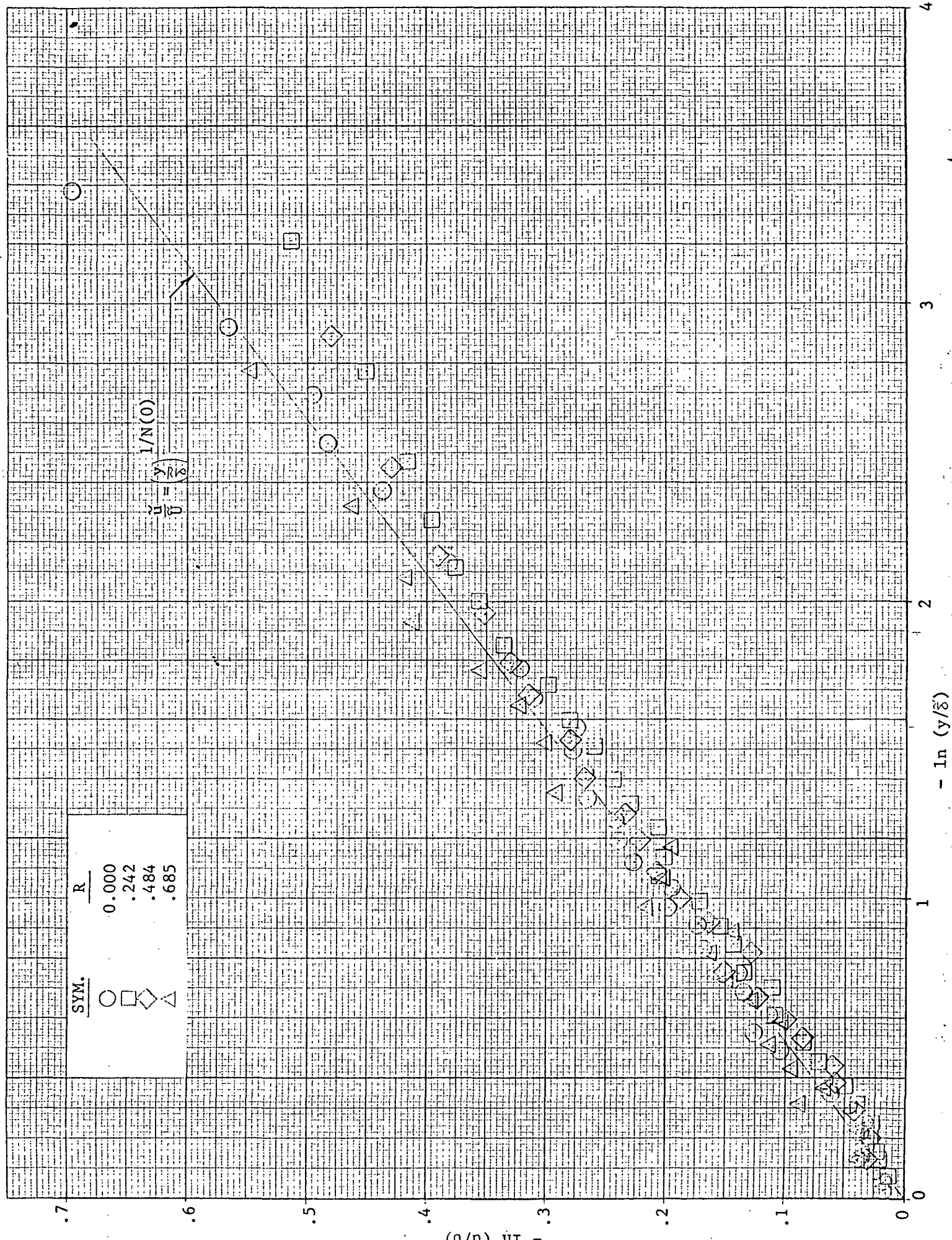

Figure 8(e).- Measured relative velocity profiles: Station x = 5.18m (17.00 ft): (concluded)

Figure 9.- Variation of n and N with belt speed

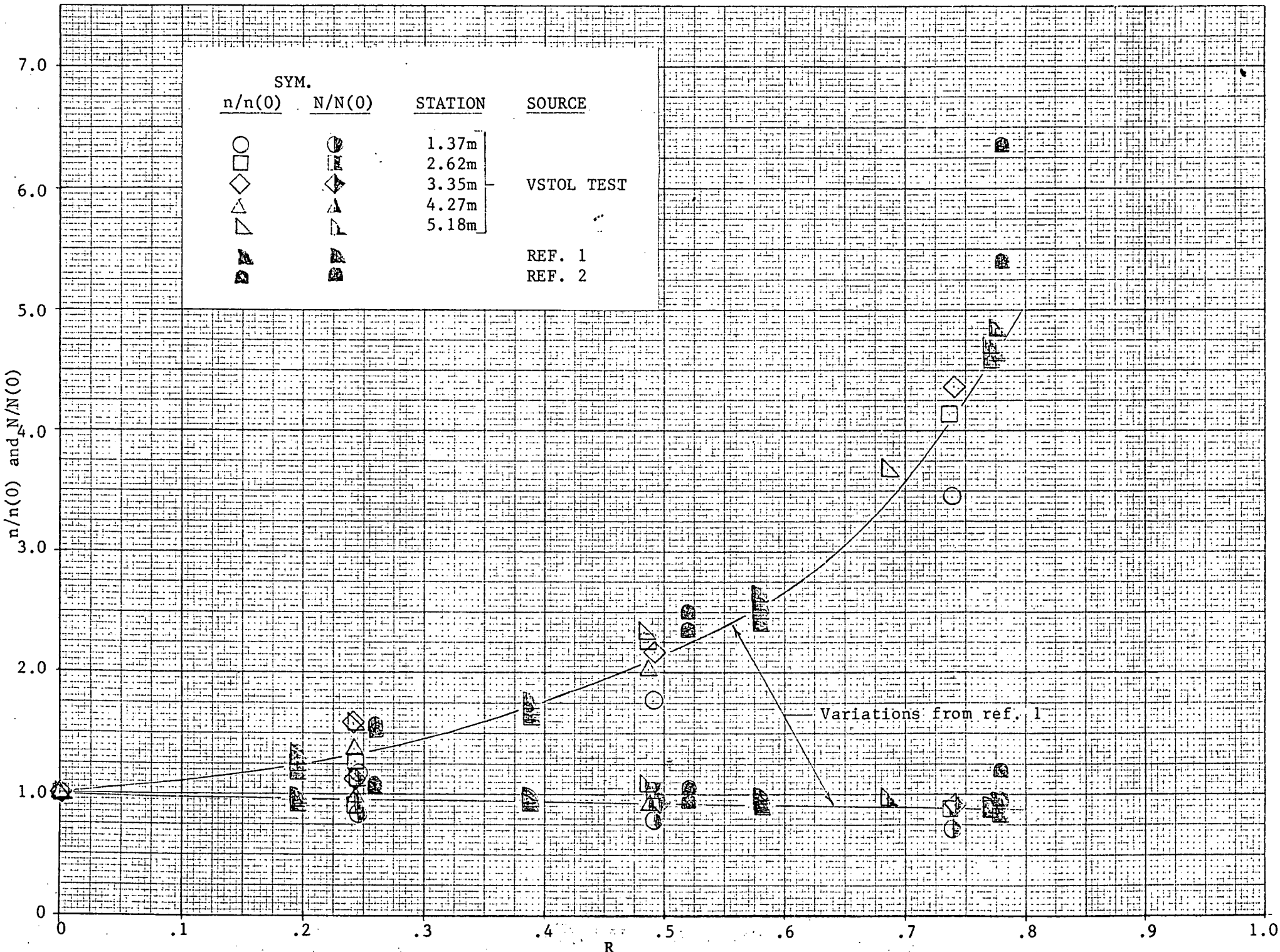

Figure 10.- Variation of relative boundary-layer thickness with ground-plane speed

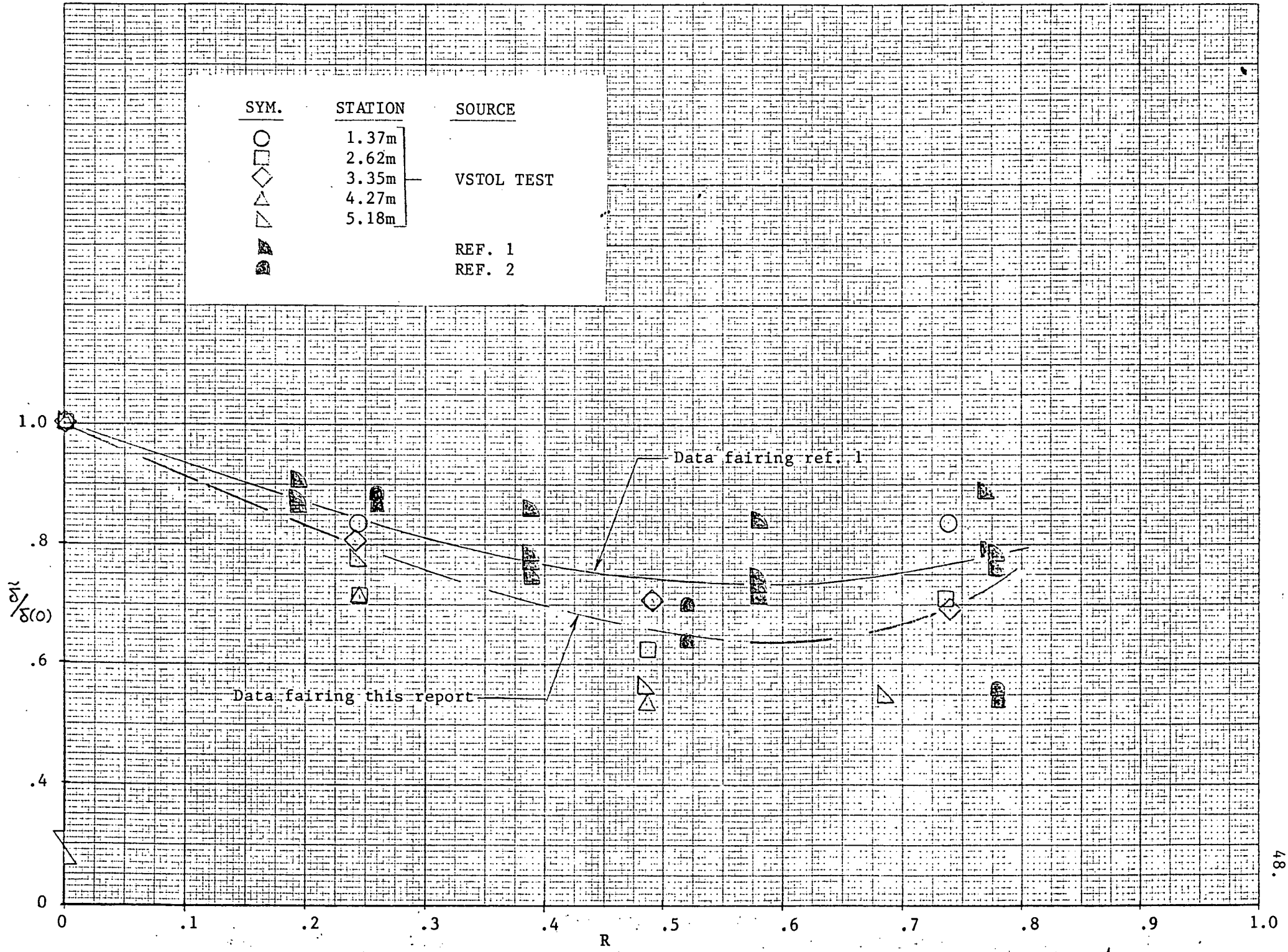

Figure 11 (a).- Comparison of measured and predicted values of the integral parameters: Station x = 1.37m (4.50 ft)

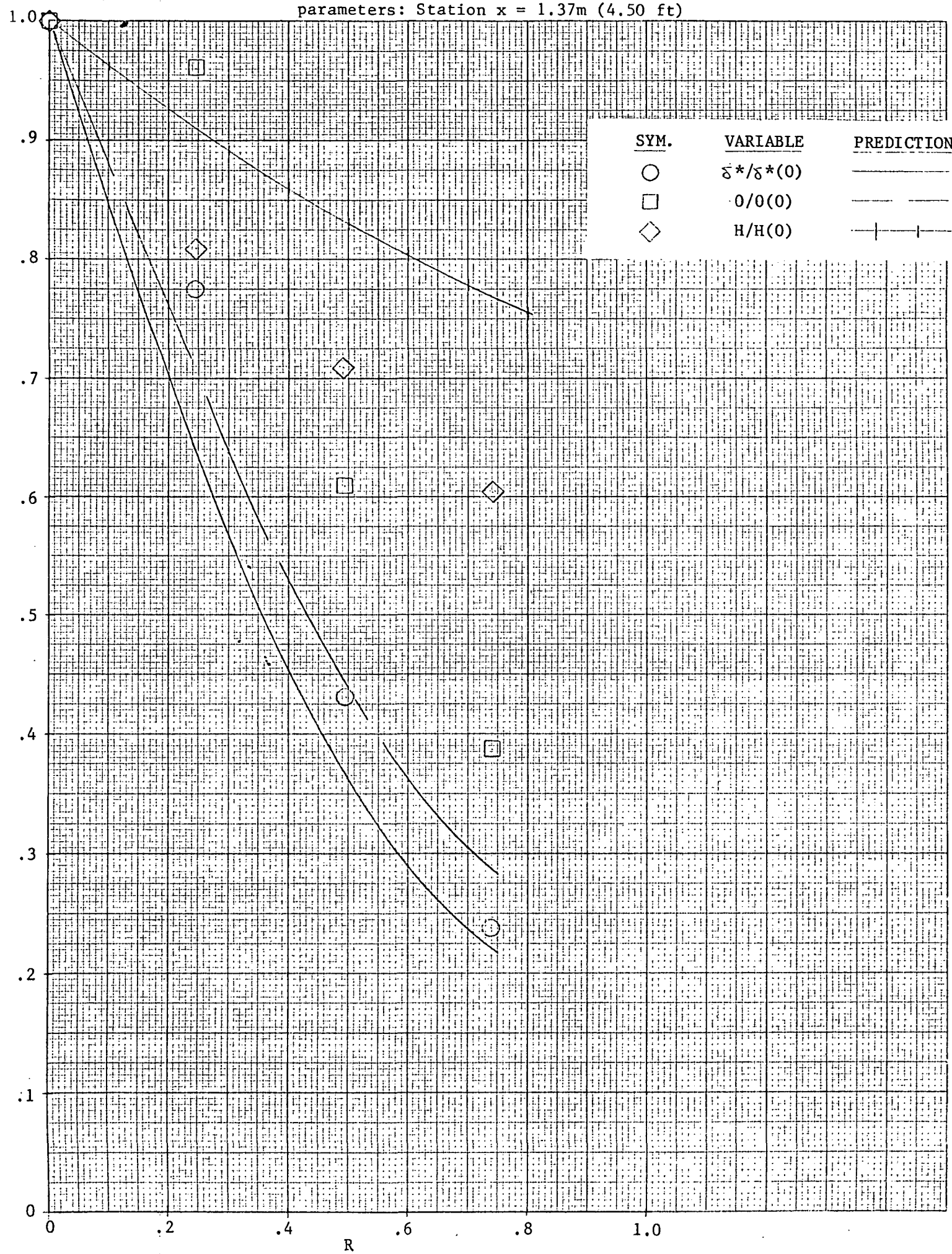

Figure 11 (b).- Comparison of measured and predicted values of the integral parameters: Station x = 2.62m (8.58 ft): (continued)

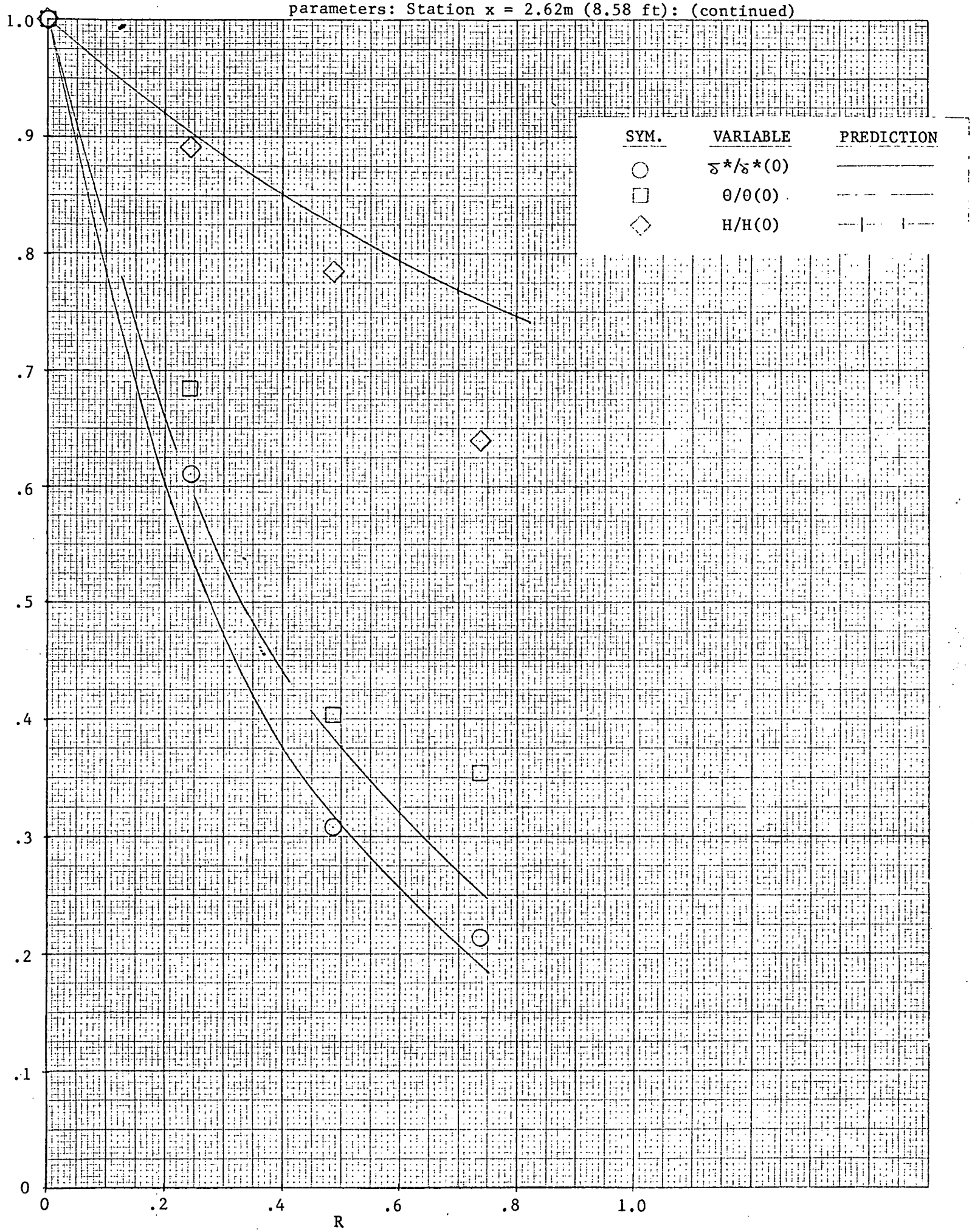

Figure 11 (c).- Comparison of measured and predicted values of the integral parameters: Station x = 3.35m (11.00 ft): (continued)

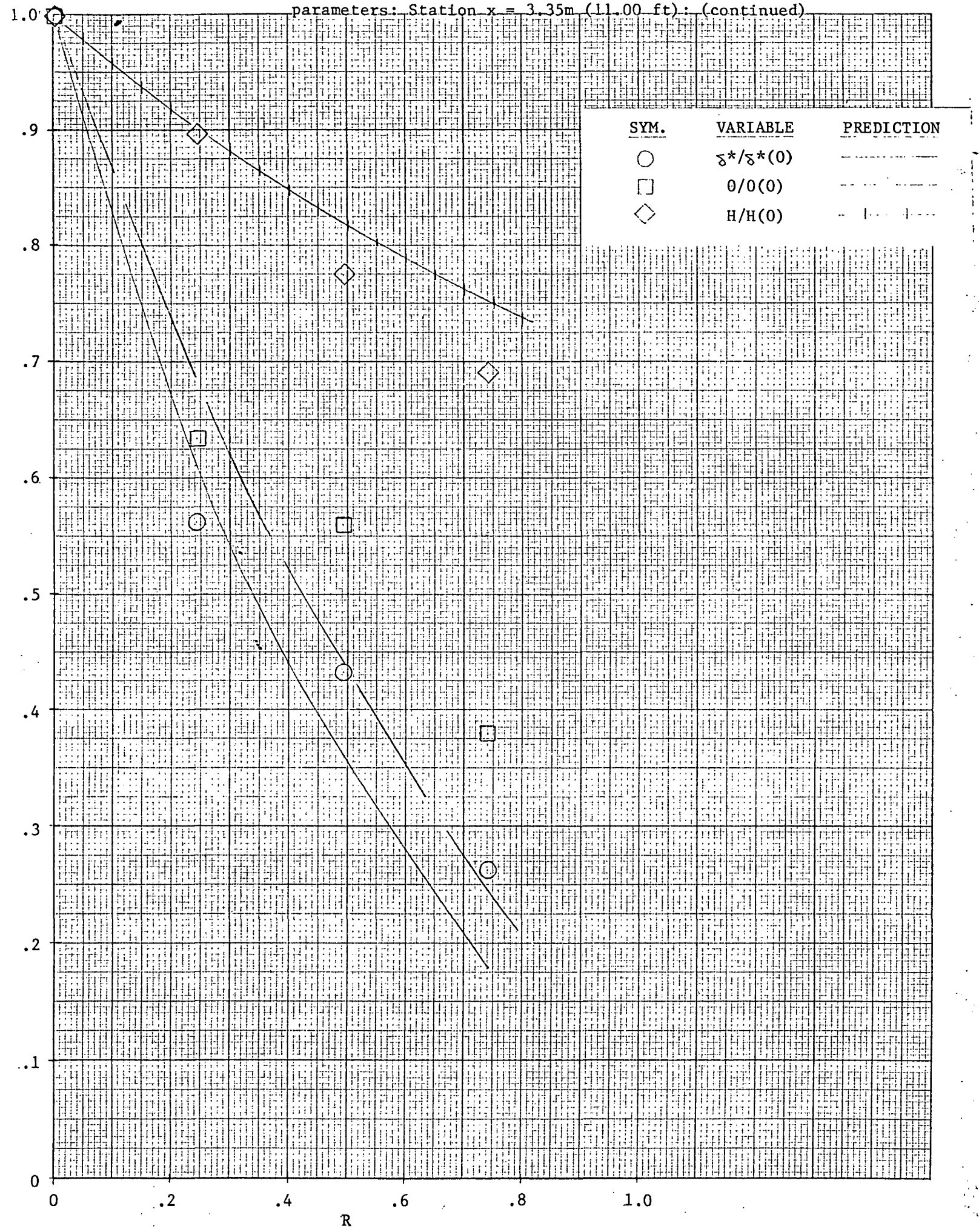

Figure 11 (d).- Comparison of measured and predicted values of the integral parameters: Station x = 4.27m (14.00 ft): (continued)

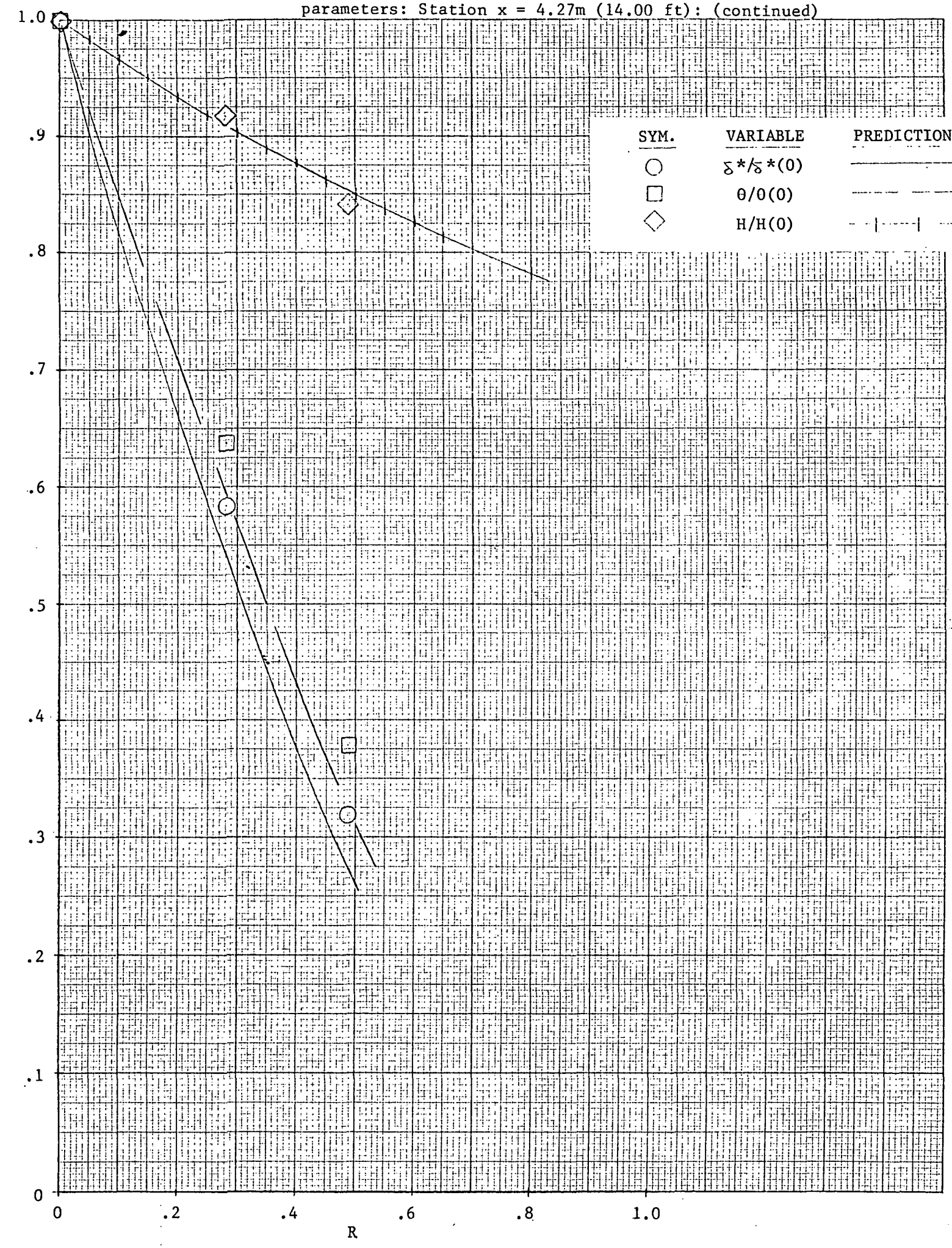

Figure 11 (e).- Comparison of measured and predicted values of the integral parameters: Station x = 5.18m (17.00 ft): (concluded)

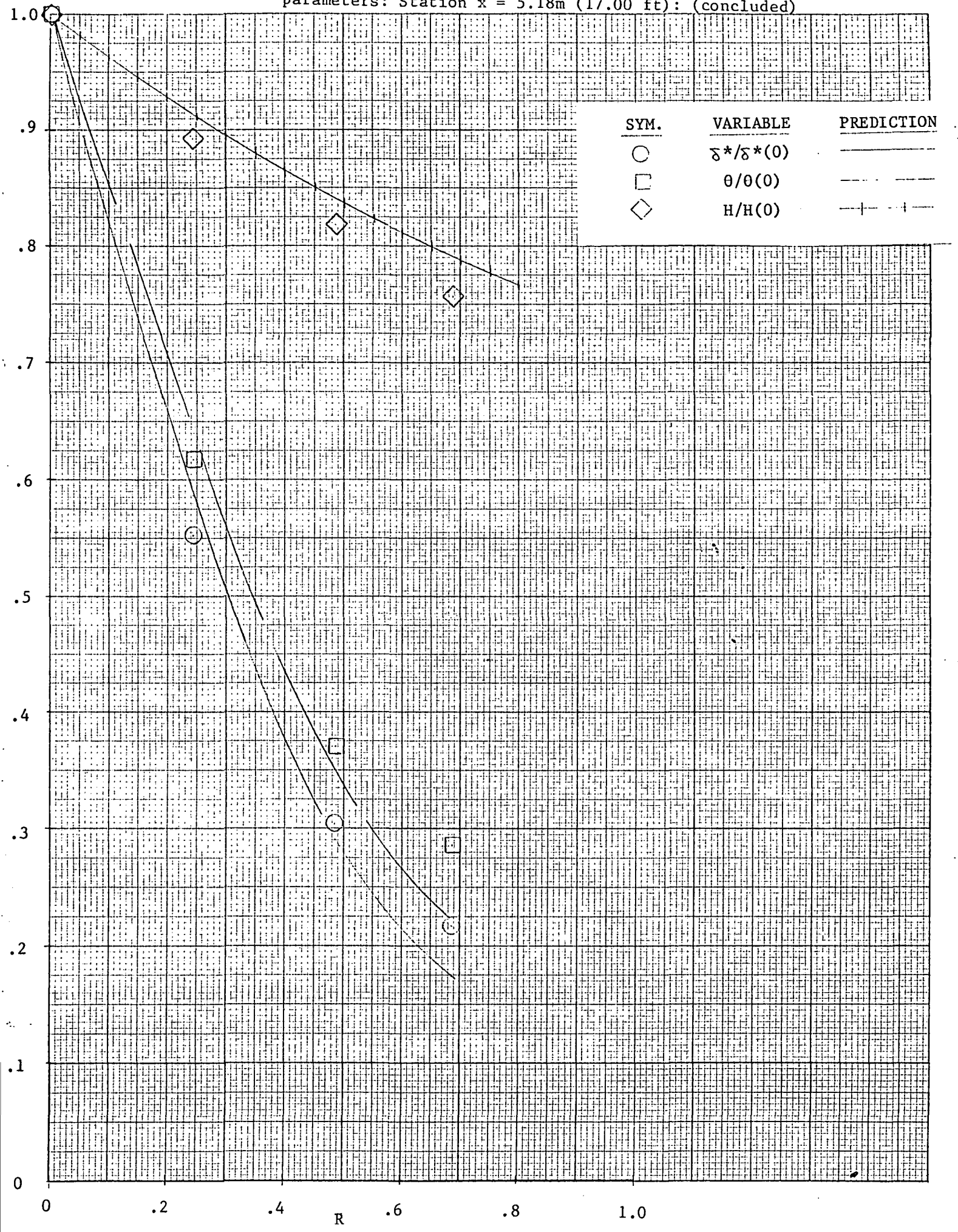

Figure 12.- Variation of the reciprocal of the exponent in the Blasius shear-stress expression as a function of the ground-plane speed

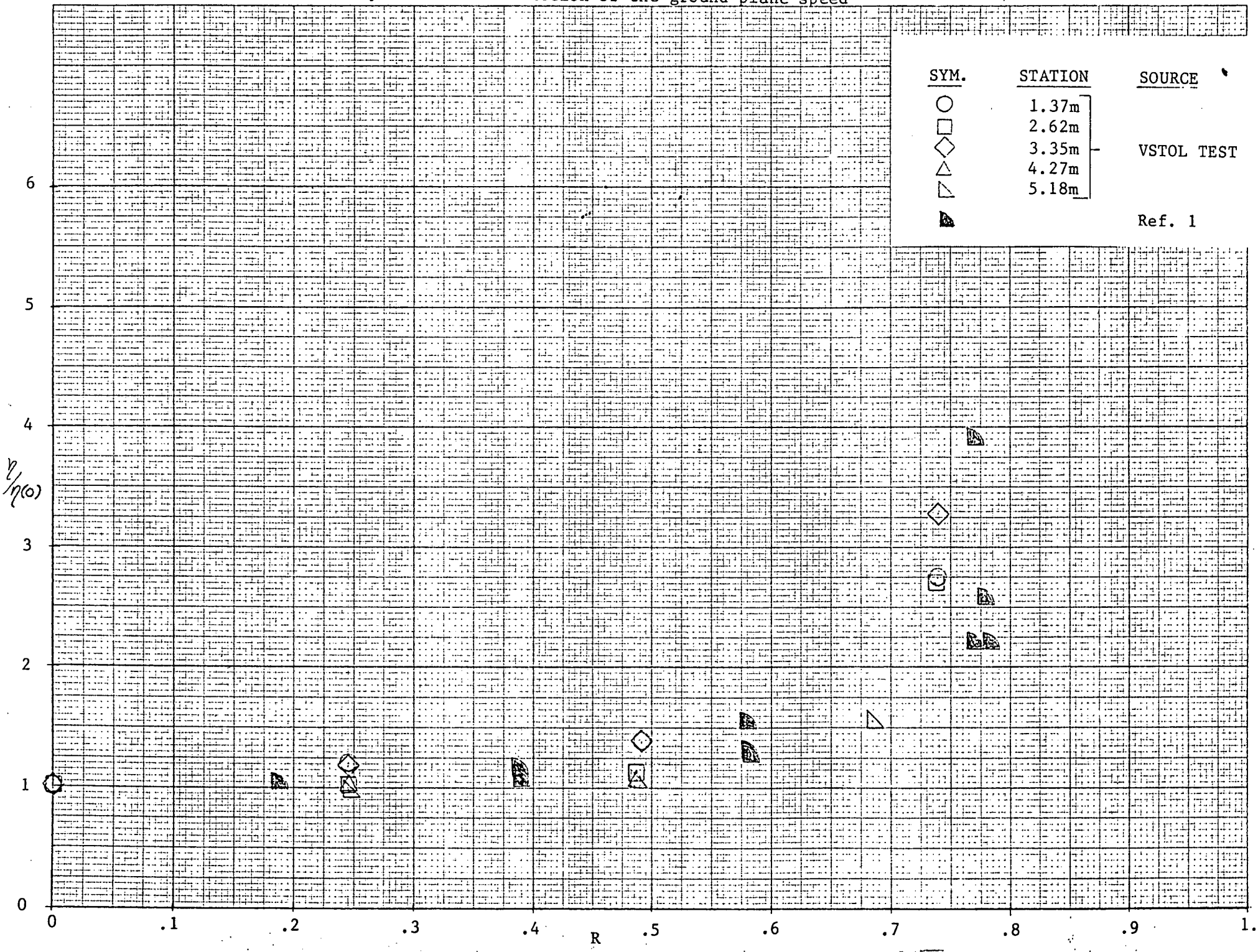

Figure 13.- Local skin-friction coefficients determined by the relative power law method

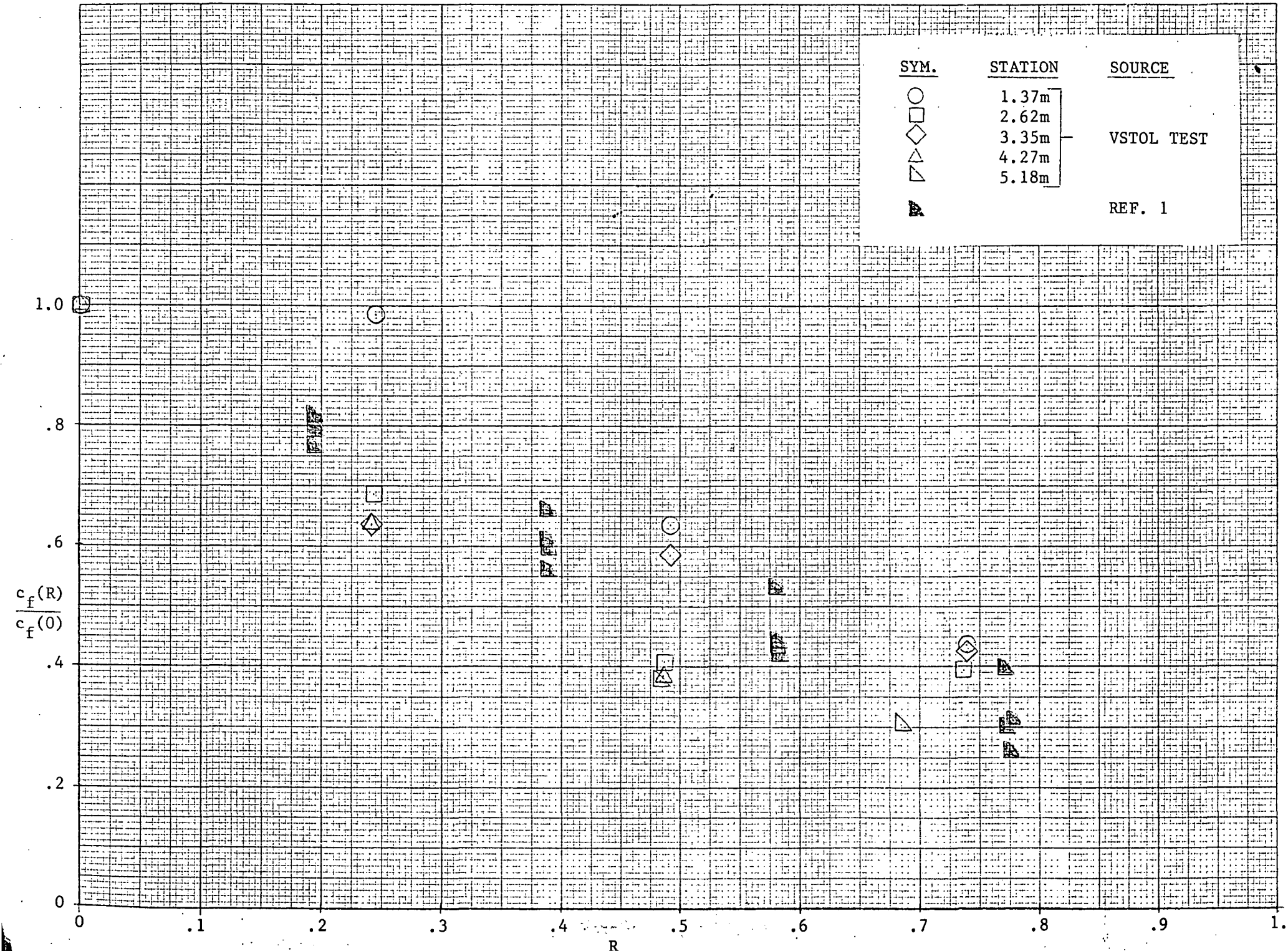

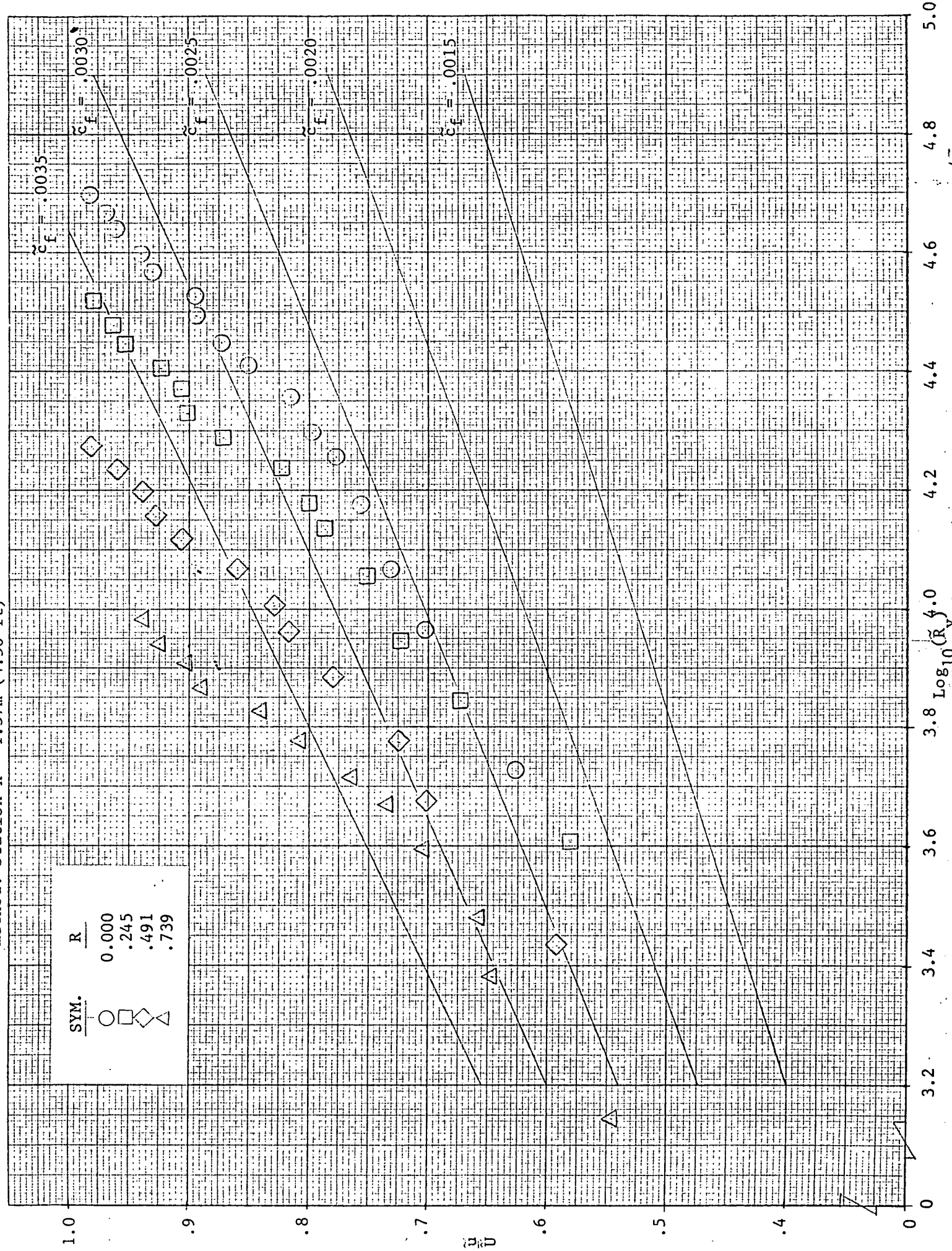

Figure 14(a).- Skin-friction coefficients determined by the modified law of the wall method: Station x = 1.37m (4.50 ft)

Figure 14(b).- Skin-friction coefficients determined by the modified law of the wall method: Station x = 2.62m (8.58 ft): (continued)

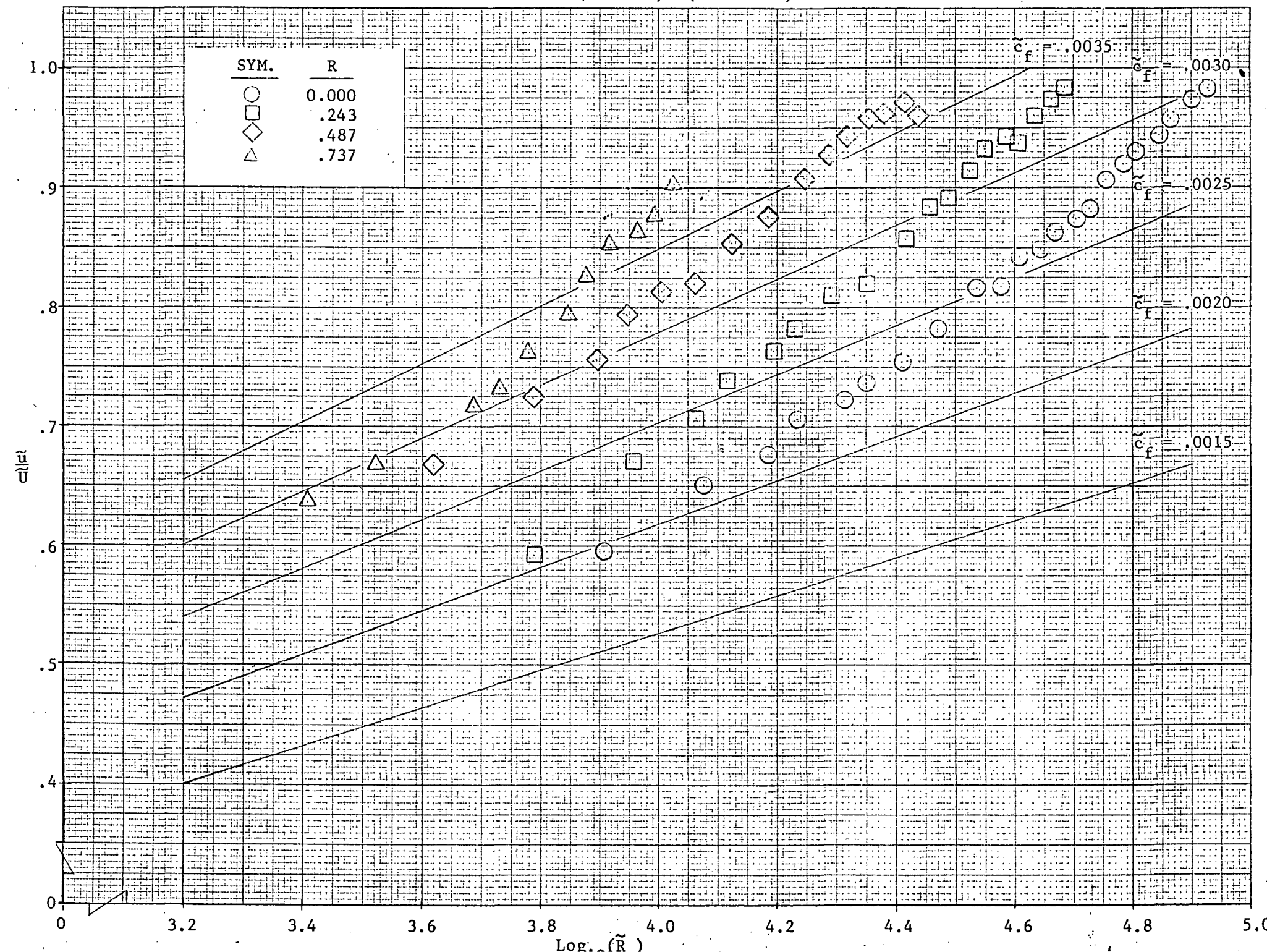

Figure 14(c).- Skin-friction coefficients determined by the modified law of the wall method: Station x = 3.35m (11 ft): (continued)

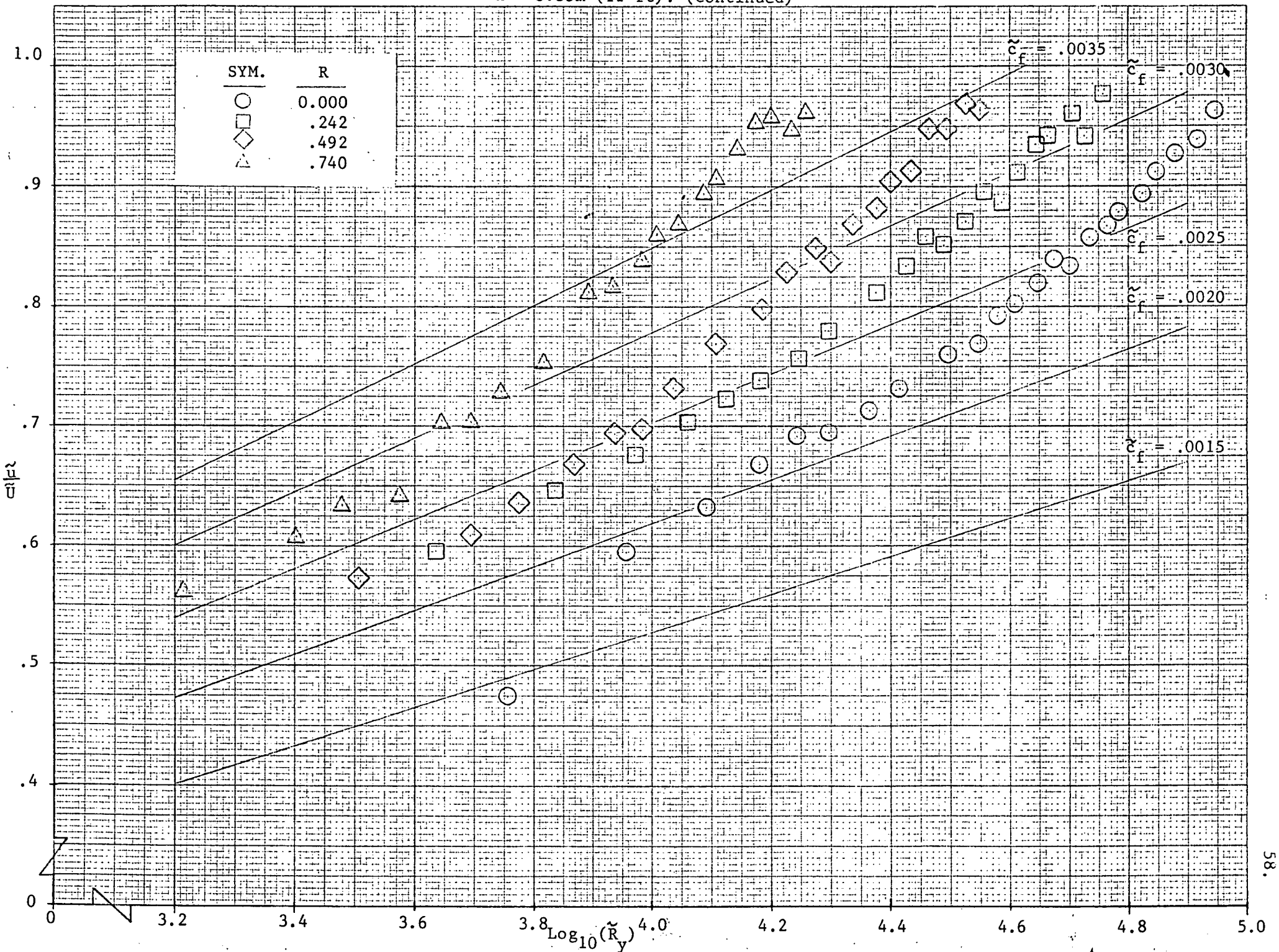

Figure 14(d).- Skin-friction coefficients determined by the modified law of the wall method: Station x = 4.27m (14.00 ft): (continued)

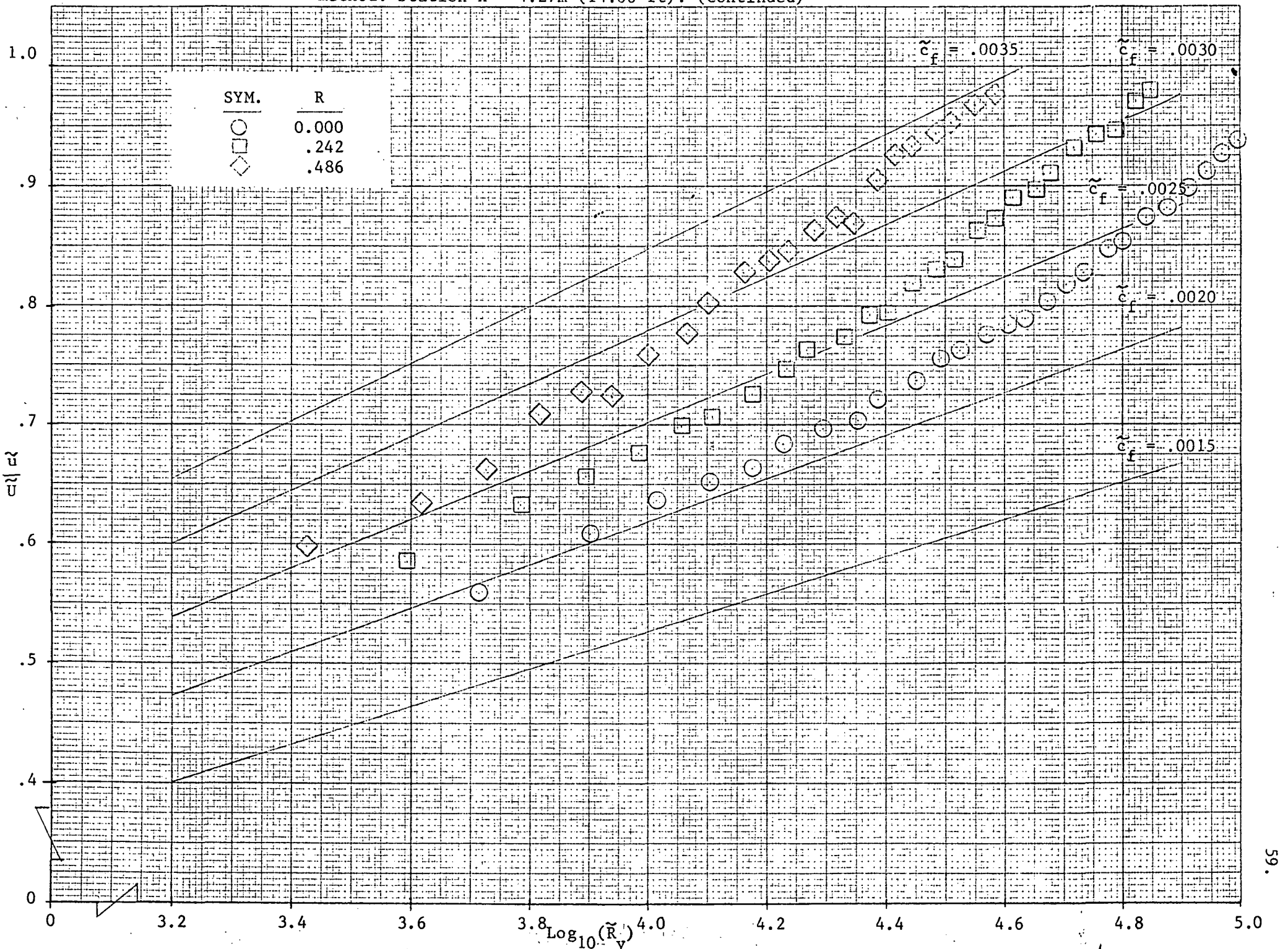

Figure 14(e).- Skin-friction coefficients determined by the modified law of the wall method: Station x = 5.18m (17.00 ft): (concluded)

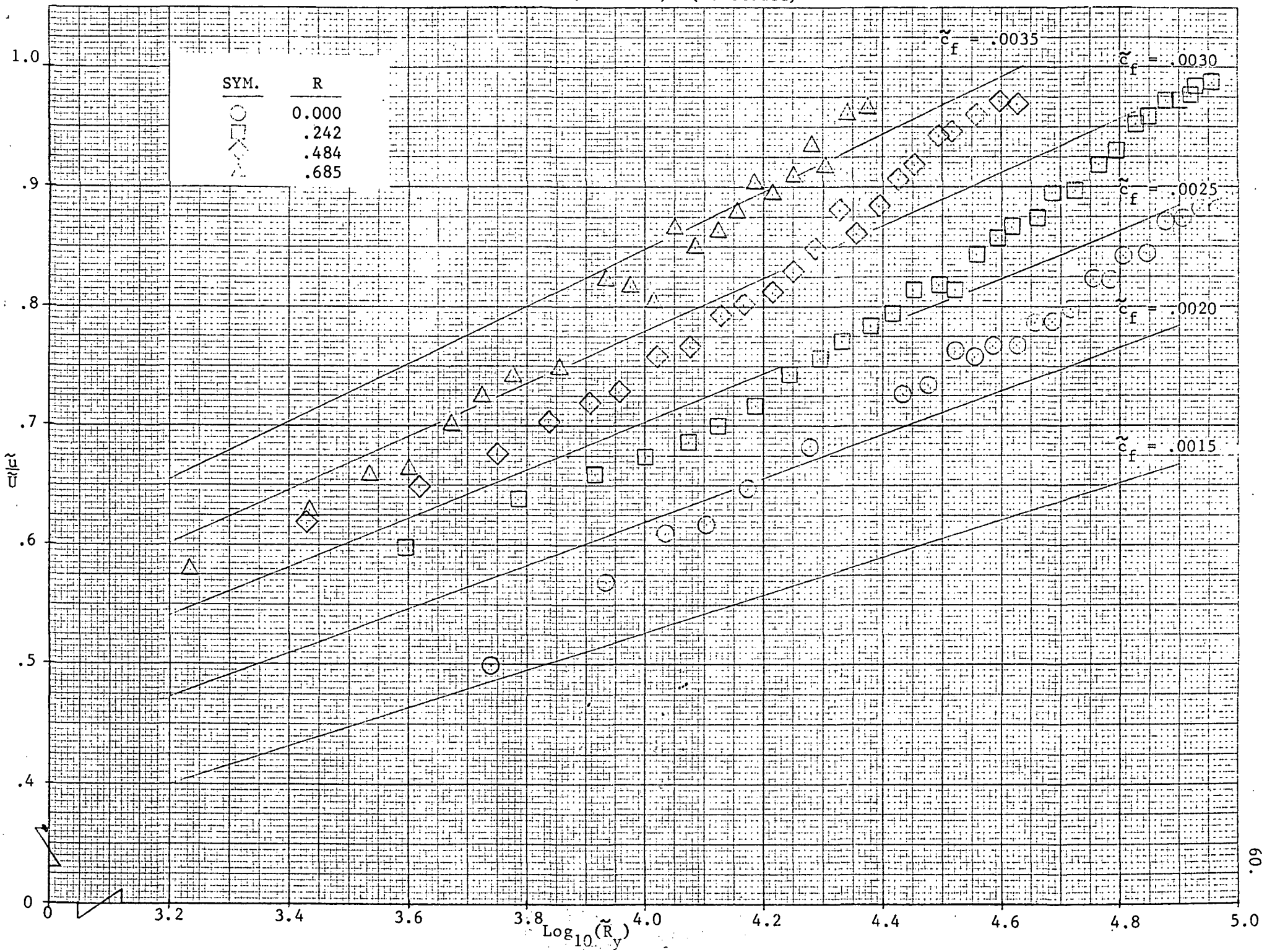

Figure 15.- Local skin-friction coefficients determined by the modified law of the wall method.

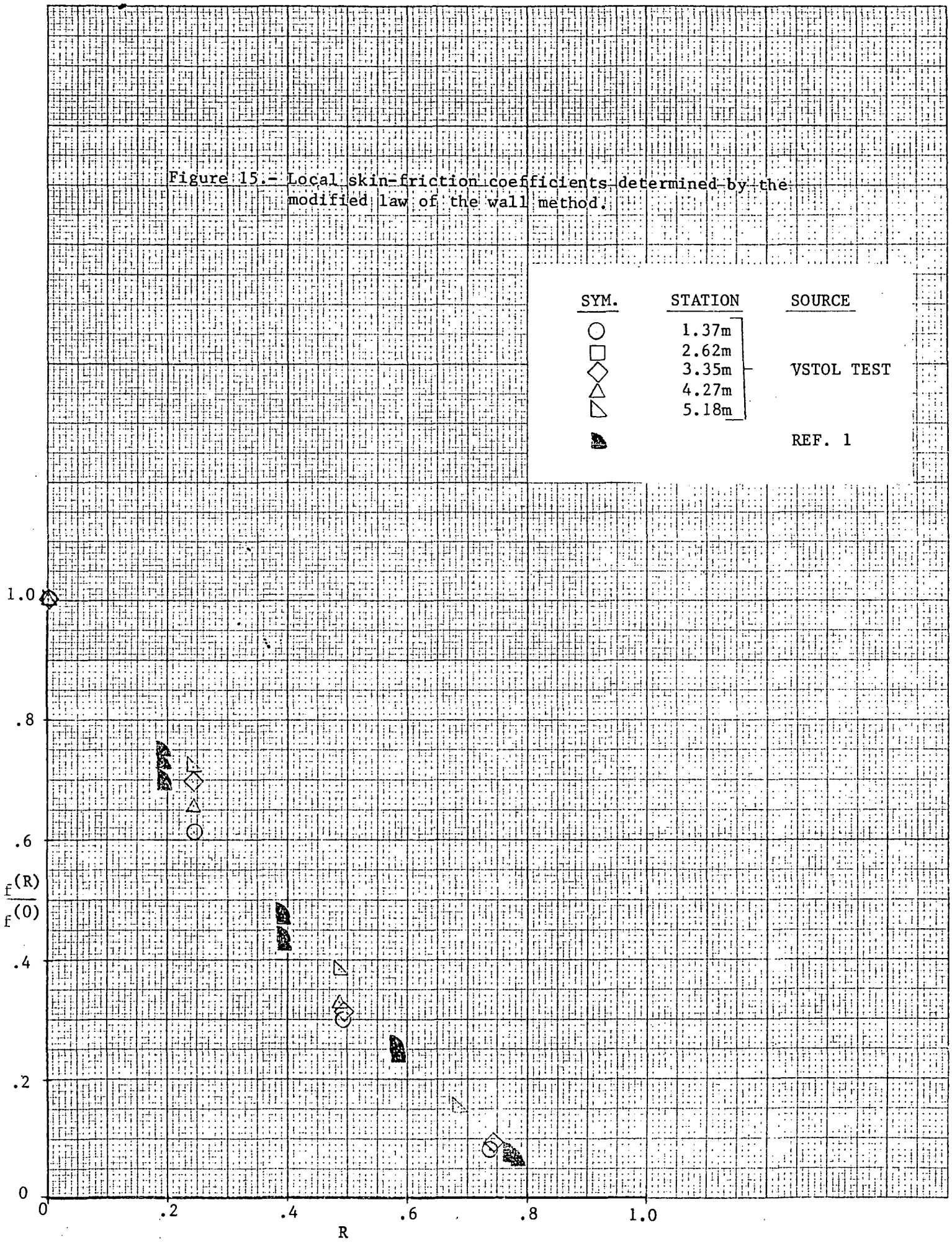

Figure 16.- Comparison of local skin-friction coefficients determined by relative integral parameter method, relative power law method, and modified law of the wall method.

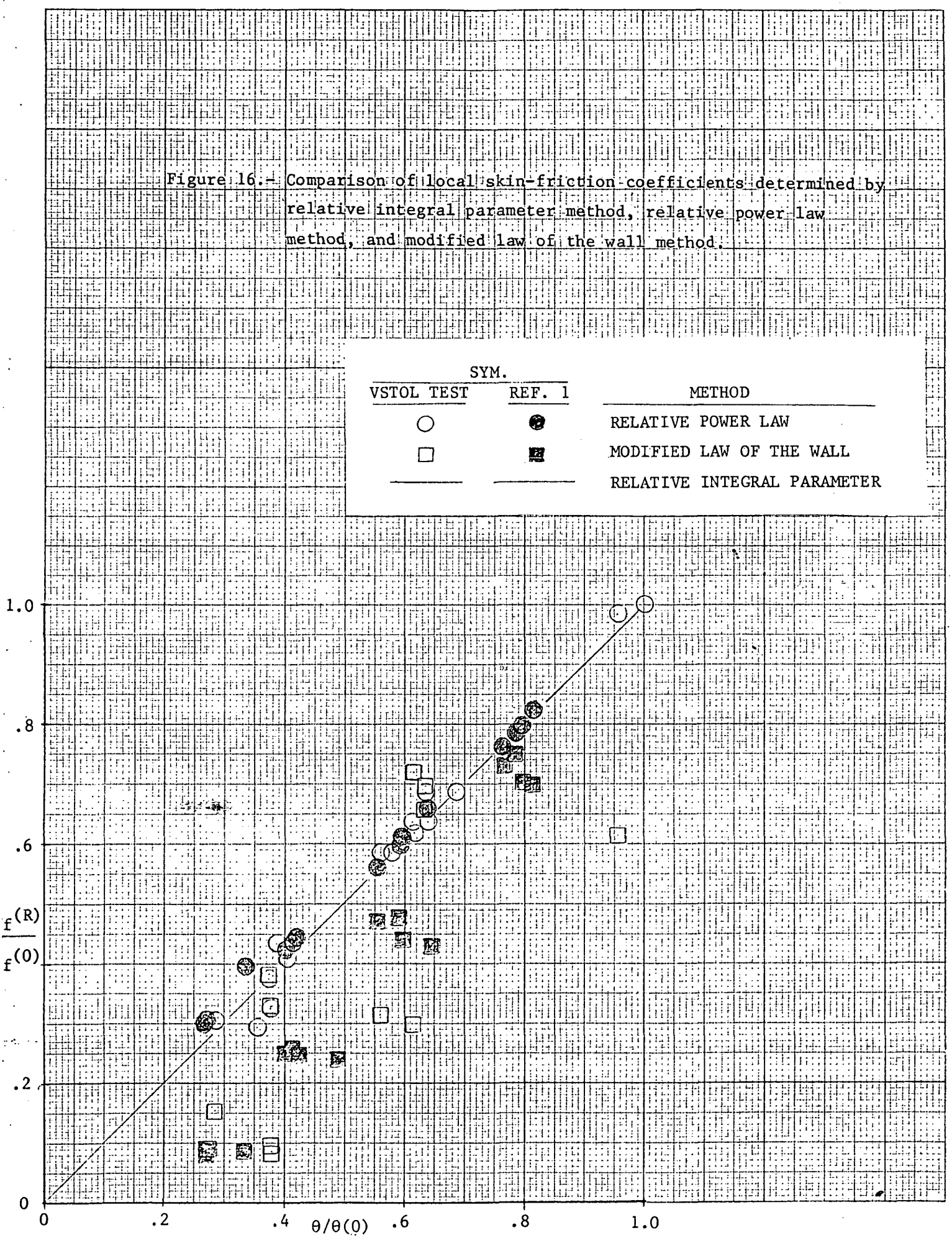

Figure 17.- Comparison of values of H(R)/H(0) predicted from the relative integral parameter, and relative power law methods with experimental data.

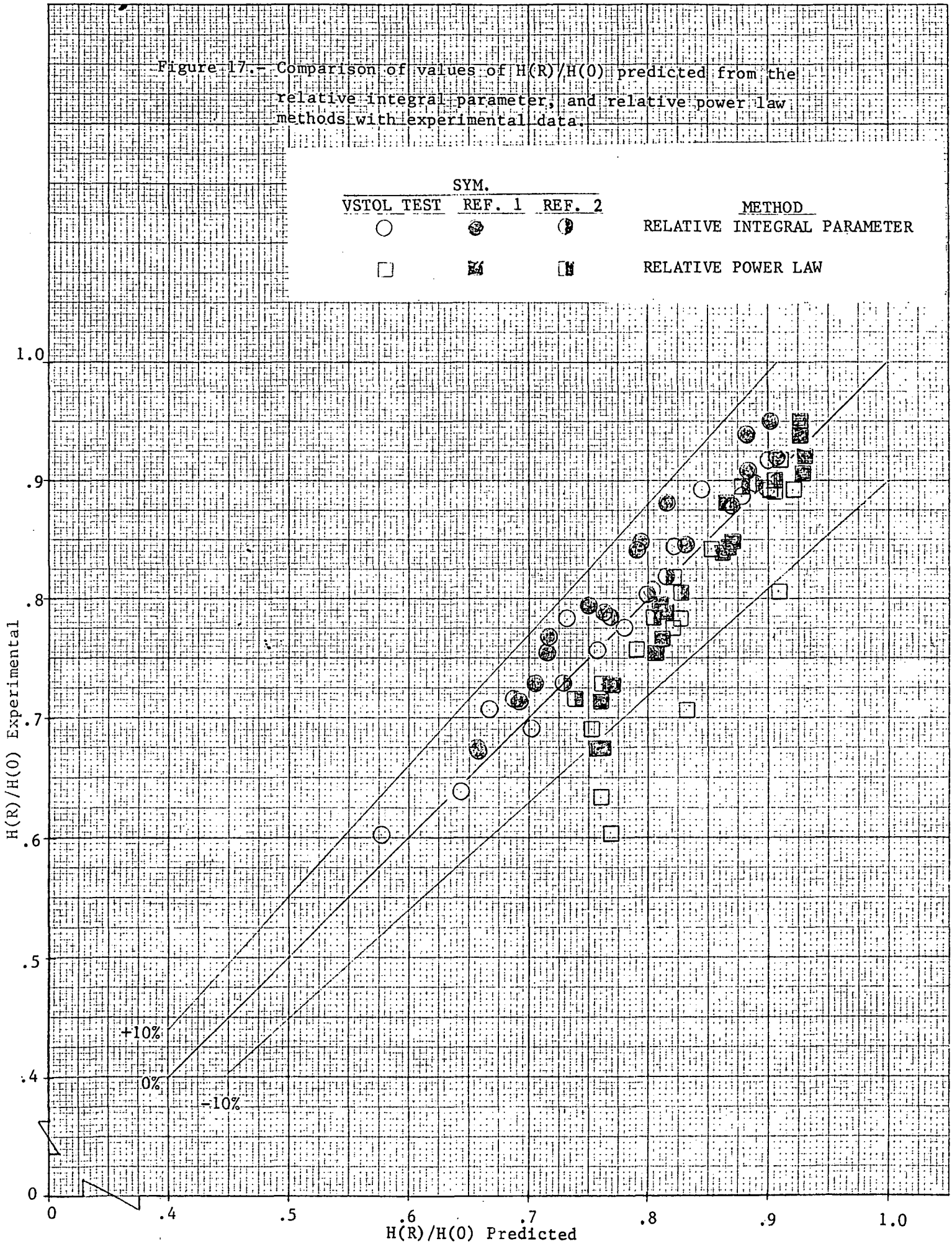

Figure 18.- Empirical variation of $\tilde{\delta}/\delta(0)$ used in relative power law computations (see Figure 10).

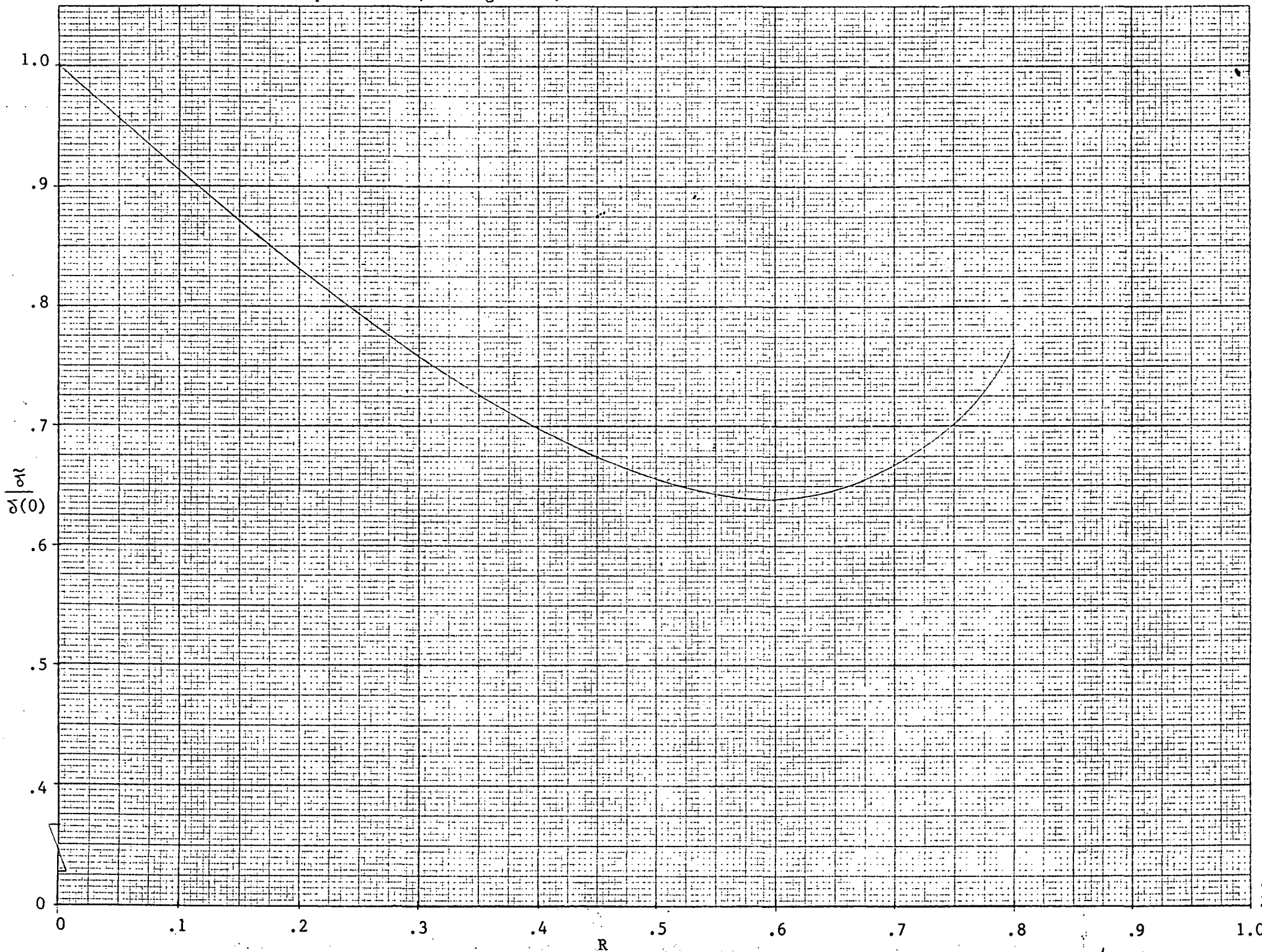

Figure 19.- Comparison of values of θ(R)/0(0) predicted from the relative integral parameter and relative power law methods with experimental data.